NASA Technical Memorandum 81284

Unpowered Aerodynamic Characteristics of a 15-Percent Scale Model of a Twin-Engine Commuter Aircraft

Daniel G. Morgan, Thomas L. Galloway, and Bruno J. Gambucci

July 1981

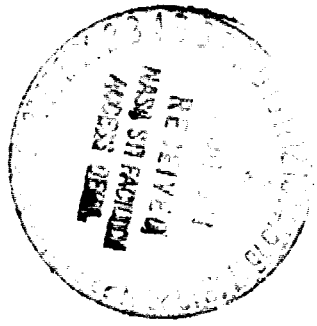

National Aeronautics and Space Administration

NASA Technical Memorandum 81284

Unpowered Aerodynamic Characteristics of a 15-Percent Scale Model of a Twin-Engine Commuter Aircraft

Daniel G. Morgan
Thomas L. Galloway, Ames Research Center, Moffett Field, California

and

Bruno J. Gambucci, Kendan Associates, Palo Alto, California

National Aeronautics and
Space Administration

Ames Research Center
Moffett Field, California 94035

NOTATION

b	wing span, m (ft)
c	wing chord parallel to plane of symmetry, m (ft)
$\bar{c}$	mean aerodynamic chord $\frac{2}{S}\int_0^{b/2} c^2\,dy$, m (ft)
c_f	flap chord
C_ℓ	rolling-moment coefficient about stability axis, $\frac{\ell}{qSb}$
C_L	lift coefficient, $\frac{L}{qS}$
C_m	pitching-moment coefficient about stability axis at $0.25\bar{c}$, $\frac{m}{qS\bar{c}}$
C_n	yawing-moment coefficient about stability axis, $\frac{n}{qSb}$
C_p	pressure coefficient
C_y	side-force coefficient about stability axis, $\frac{y}{qS}$
D	drag, N (lb)
i_t	horizontal-tail incidence angle, deg
ℓ	rolling moment, N-m (ft-lb)
L	total lift on model, N (lb)
m	pitching moment, N-m (ft-lb)
M	Mach number
n	yawing moment, N-m (ft-lb)
p_o	Standard absolute pressure, 101352.9 N/m^2 (14.7 psi)
p_s	freestream static pressure, N/m^2 (psf)
q	freestream dynamic pressure, N/m^2 (psf)
S	wing area, m^2 (ft^2)
y	side force, N (lb)
α	angle of attack, deg
β	angle of sideslip, deg

δ_f trailing-edge flap deflection, deg

Subscripts:

f flap

s static conditions

t tail

u uncorrected data

UNPOWERED AERODYNAMIC CHARACTERISTICS OF A 15-PERCENT-SCALE MODEL OF A TWIN-ENGINE COMMUTER AIRCRAFT

Daniel G. Morgan, Thomas L. Galloway, and Bruno J. Gambucci*

Ames Research Center

SUMMARY

An experimental investigation was conducted in the Ames 12-Foot Pressure Wind Tunnel to determine the unpowered aerodynamic characteristics of a 15-percent-scale model of a twin-engine commuter aircraft. Model longitudinal aerodynamic characteristics were examined at discrete flap deflections for various angle-of-attack and wind-tunnel-velocity ranges with the empennage on and off. Lateral-directional data were obtained for a range of sideslip angles at model angles of attack of 0°, 4°, and 8°. The Reynolds number was varied from 0.518×10^6/m (1.7×10^6/ft) to 2.134×10^6/m (7.0×10^6/ft). Lateral directional characteristics were examined at a Reynolds number of 1.646×10^6/m (5.4×10^6/ft).

Data are presented for the basic model configuration consisting of the fuselage, wing, basic wing leading edge, double slotted flaps, midengine nacelles, and empennage. Other configurations tested include a partial-span drooped leading edge (drooped outboard of the engine nacelles), a full-span drooped leading edge, low- and high-mounted engine nacelles, and a single-slotted flap. Some data were also obtained of flow visualization, fixed boundary-layer transition on the wing leading edge, and the wing pressure distribution.

An evaluation was made of the model mounting system by comparing data obtained with the model mounted conventionally on the wind-tunnel model-support struts and the model inverted.

INTRODUCTION

In the past, the aerodynamic technology utilized on commuter-type aircraft reflected mainly past research and development efforts of the large-transport aircraft manufacturers. However, since the large-transport aircraft manufacturers have developed larger jet transports, the technology is generally no longer suitable for application to small, short-haul transport aircraft. The nature of the compromise between performance and cost for these small, short-haul aircraft differs from that for large, long-range, high-speed, jet-transport aircraft.

---

*Senior Associate, Kendan Associates, Palo Alto, California 94303.

TABLE 1.- MODEL DIMENSIONAL DATA

Complete model		
Volume, m^3 (ft^3)	0.12997	(4.59)
Area, m^2 (ft^2)	.16537	(1.78)
Overall length, m (ft)	2.7137	(8.90)
Wing		
Volume, m^3 (ft^3)	.01359	(0.48)
Area, m^2 (ft^2)	.57971	(6.24)
Span, m (ft)	2.1143	(6.937)
Aspect ratio		7.71
Chord, m (ft)		
Root	.39268	(1.288)
Tip	.15646	(0.5133)
Mean aerodynamic chord, $\bar{c}$, m (ft)	.2?134	(0.956)
Airfoil section (NACA), m (ft)		
Root		65_2A215
Tip		64_2A415
Distance from centerline to $\bar{c}$, m (ft)	.43409	(1.424)
Taper ratio		.398
Sweep at leading edge, deg		4.5
Sweep at 25% chord, deg		.9
Sweep-flap leading edge, deg		-6.0
Sweep at trailing edge, deg		-9.0
Root incidence, deg		1.0
Tip incidence, deg		-1.0
Dihedral, deg		5.0
Flap span, m (ft)	.54864	(1.80)
Aileron span, m (ft)	.35966	(1.18)
Fuselage		
Volume, m^3 (ft^3)	.10166	(3.59)
Volume nose cone, m^3 (ft^3)	.01586	(0.56)
Volume tail cone, m^3 (ft^3)	.01303	(0.46)
Volume cylinder, m^3 (ft^3)	.07334	(2.59)
Diameter, m (ft)	.25146	(0.825)
Length, m (ft)	2.62738	(8.62)
Horizontal tail		
Volume, m^3 (ft^3)	.00198	(0.07)
Area, m^2 (ft^2)	.15143	(1.63)
Span, m (ft)	.73660	(2.417)
Aspect ratio		3.58
Chord, m (ft)		
Root	.30480	(1.00)
Tip	.14122	(0.463)
Mean aerodynamic chord, $\bar{c}$, m (ft)	.24257	(0.796)
Airfoil section (NACA), m (ft)		
Root		66A009
Tip		63A009
Distance from centerline to $\bar{c}$, m (ft)	.14300	(0.469)
Taper ratio		0.463

TABLE 1.- CONCLUDED

Horizontal tail (concluded)	
Sweep at leading edge, deg	39.0
Sweep at 25% chord, deg	34.5
Sweep at trailing edge, deg	15.5
Vertical tail	
Volume, m^3 (ft^3)	0.00255 (0.09)
Area, m^2 (ft^2)	.08826 (0.95)
Span, m (ft)	.43180 (1.417)
Chord, m (ft)	
Root	.31750 (1.042)
Tip	.14122 (0.463)
Mean aerodynamic chord, $\bar{c}$, m (ft)	.24638 (0.808)
Airfoil section (NACA), m (ft)	
Root	66A009
Tip	63A009
Distance from centerline to $\bar{c}$, m (ft)	.23876 (0.783)
Sweep at leading edge, deg	39.0
Sweep at 25% chord, deg	34.5
Sweep at rudder leading edge, deg	20.0
Sweep at trailing edge, deg	15.5
Miscellaneous	
Nacelle volume, m^3 (ft^3)	.01048 (0.37)
Thrust incidence, deg	0.0

Wing

The aspect ratio of the wing was 7.71, the taper ratio 0.398, and the sweep along the quarter-chord line 0.9°. The leading-edge and trailing-edge sweeps of the wing were 4.5° and -9.0°, respectively. The wing section at the root was the NACA 65_2A215 section and at the tip, the NACA 64_2A415 section. The incidence was 1.0° at the wing root and -1.0° at the tip. Wing airfoil coordinates are presented in table 2. The leading and trailing edges were removable so that an alternate drooped-leading-edge configuration or single-slotted-flap trailing-edge configuration could be installed. Two drooped-leading-edge configurations were used; one had a drooped leading edge extending outboard of the engine nacelles (partial-span drooped-leading-edge configuration) and the other was drooped the full spanwise extent of the wing leading edge. A typical cross section and ordinates for the drooped-wing leading edge are presented in figure 6(a).

Flaps and Ailerons

For this investigation the ailerons were not deflected. The basic flap configuration was the double-slotted flap. Flap deflections were positioned by brackets for discrete deflections of 0°, 18°, 36°, and 54°. Also

TABLE 2.- AIRFOIL COORDINATES AT WING STATION 0.1052 m (4.14 in.)

(Wing root)

Upper surface		Lower surface	
x/c	y/c	x/c	y/c
0.0	0.00622		
.00208	.01373	0.00206	-0.00129
.00694	.01992	.00687	-.00650
.02028	.02887	.01890	-.01408
.02974	.03367	.02852	-.01784
.05454	.04282	.05233	-.02489
.07927	.05034	.07601	-.03076
.12830	.06199	.12353	-.03997
.17697	.07046	.17128	-.04704
.22536	.07694	.21944	-.05260
.27359	.08158	.26720	-.05689
.32156	.08486	.31501	-.06022
.37121	.08670	.36312	-.06225
.41794	.08688	.41140	-.06331
.46564	.08561	.46029	-.06302
.51479	.08250	.50907	-.06128
.56365	.07764	.55764	-.05826
.61278	.07118	.60668	-.05405
.66190	.06371	.65508	-.04910
.71071	.05502	.70388	-.04371
.75915	.04541	.70683	-.04332
.80776	.03494	.70956	-.04296
.85609	.02363	.75606	-.03739
.90559	.01204	.80397	-.03172
.95321	.00061	.85124	-.02643
1.0	-.01065	.89775	-.02169
		.94426	-.01676
		.99105	-.01192
		.99367	-.01169
		.99578	-.01153
		1.0	-.01123

(Wing tip)

Upper surface		Lower surface	
x/c	y/c	x/c	y/c
0.0	0.0	0.0	0.0
.00277	.01284	.00723	-.01060
.00501	.01573	.00999	-.01256
.00967	.02034	.01533	-.01552
.02168	.02908	.02832	-.02064
.04625	.04178	.05375	-.02735
.07109	.05157	.07891	-.03211
.09606	.05975	.10394	-.03590
.14621	.07281	.15390	-.04158
.19655	.08274	.20345	-.04553
.24699	.09022	.25301	-.04817
.29750	.09563	.30250	-.04969
.34806	.09908	.35194	-.05012
.39865	.10043	.40135	-.04928
.44925	.09941	.45075	-.04684
.49983	.09638	.50017	-.04318
.55037	.09169	.54963	-.03864
.60084	.08559	.59916	-.03352
.65125	.07819	.64875	-.02800
.70158	.06962	.69842	-.02232
.75185	.06003	.74815	-.01682
.80222	.04945	.79778	-.01207
.85127	.03754	.84783	-.00868
.90152	.02531	.89848	-.00570
.95078	.01282	.94922	-.00301
1.0	.00032	.99997	-.00320

investigated was a single-slotted flap. Typical cross sections of the two flap configurations are shown in figure 6(b).

Nacelles

Engine nacelles with the same geometric details were investigated; they were mounted in three positions with respect to the wing. The basic configuration was with the nacelle in the midposition. Alternate positions were overwing (high nacelle) and underwing (low nacelle). Nacelle details are

shown in figure 6(c). Photographs of the model with the nacelles in the different positions are presented in figure 7.

Empennage

The horizontal tail had an NACA 66A009 airfoil section at the root and an NACA 63A009 airfoil section at the tip. The aspect and taper ratios of the tail were 3.58 and 0.463, respectively. The horizontal tail was movable and could be actuated remotely over an incidence range of -8° to 8°.

The vertical tail also had an NACA 66A009 airfoil section at the root and an NACA 63A009 airfoil section at the tip; the rudder was not deflected. Because the model was designed for the empannage to be removable, data were also obtained with the horizontal and vertical sections removed.

TESTS AND PROCEDURE

Longitudinal force and moment data were obtained at discrete flap deflections for model angles of attack through stall and for various wind-tunnel velocities. Tests were made with the empennage on and off. Lateral-directional data were obtained for a range of sideslip angles at model angles of attack of 0°, 4°, and 8°. Tail incidence sweeps were also made at model angles of attack of 0°, 4°, and 8°. A summary of the principal test variables is presented in the following tables:

Model parameter	Range, deg
α_u	-4 to 17
δ_f	0, 18, 36, 54
i_t	-8 to 8
β	-2 to 6

Wind tunnel					
Reynolds number		Stagnation pressure		Dynamic pressure	
$\cdot 10^6$/m	($\times 10^6$/ft)	N/m^2	(psi)	N/m^2	(psf)
0.518	(1.7)	101353	(14.7)	4309	(90)
1.646	(5.4)	275790	(40.0)	19630	(410)
1.219	(4.0)	413685	(60.0)	6703	(140)
1.646	(5.4)	413685	(60.0)	11730	(245)
2.103	(6.9)	413685	(60.0)	22503	(470)

In order to evaluate the effects of the model mounting system, data were also obtained with the model mounted in an inverted position, as shown in figure 2. With the model inverted, positive pitch was limited to 10° and, therefore, maximum lift could not be defined. Also, the model configurations were limited to tail off because of the interference effects of the strut.

For the flow-visualization studies, microtufts were placed on the upper-right-wing surface of the model. Tufts were also placed on the right-engine nacelle. Photographs of the tufts were made for the wing-body configuration with the nacelles removed and with the mid and high nacelles at flap deflections of 0° and 36°.

In order to determine the effects of transition, carborundum grit was placed on the model wing, nose, and tail to form transition strips. The transition strips, made of number 60 carborundum grit, were placed spanwise on the upper and lower surfaces of the wing at the 10- and 15-percent wing-chord stations. The transition strips were 0.64 cm (0.25 in.) wide. Transition strips also were mounted on the 10- and 15-percent chord stations on the upper and lower surfaces of the horizontal tail. Transition on the vertical tail was located at 10-percent chord on both surfaces. The fuselage transition was placed 6.35 cm (2.5 in.) from the nose.

Wing pressure distributions were measured by using two pressure straps. The straps were made of ten 0.0762-cm-diameter (0.030-in.) stainless-steel tubes soldered together side by side and bent to the contour of the wing. The tubes were plugged near the leading edge of the wing so that each tube served a dual purpose (upper- and lower-surface measurements). Photographs of the pressure-strap installation are shown in figure 8. One pressure strap was mounted outboard of the right nacelle and the other inboard of the left nacelle. The spanwise position and chordwise orifice locations are indicated in Table 3. Pressure data were obtained with the midnacelles on and off the wing.

The wing-body fairing on the basic model configuration was referred to as the long fairing. In order to determine the effects of fairing size, a much shorter wing-body fairing was also investigated. Details of the two fairings are shown in the photographs in figure 9.

TABLE 3.- PRESSURE-STRAP ORIFICE LOCATION

Pressure tap no.	Left-wing strap,[a] x/c	Pressure tap no.	Right-wing strap,[b] x/c
1	0.0 L.E.[c]	21	0.0 L.E.[c]
2	.05 U.S.[d]	22	.05 U.S.[d]
3	.10	23	.10
4	.15	24	.15
5	.20	25	.20
6	.30	26	.30
7	.40	27	.40
8	.50	28	.50
9	.70	29	.70
10	.90	30	.90
11	1.00 T.E.[e]	31	1.00 T.E.[e]
12	.05 L.S.[f]	32	.05 L.S.[f]
13	.10	33	.10
14	.15	34	.15
15	.20	35	.20
16	.30	36	.30
17	.40	37	.40
18	.50	38	.50
19	.70	39	.70
20	.90	40	.90

[a]Left-wing pressure strap is located 22.5 cm () in.) spanwise from fuselage centerline.

[b]Right-wing pressure strap is located 45 cm (18 in.) spanwise from fuselage centerline.

[c]Leading edge.

[d]Upper surface.

[e]Trailing edge.

[f]Lower surface.

DATA CORRECTIONS

Force and moment data were corrected for wind-tunnel wall constraints in the following manner:

$$\alpha = \alpha_u + 0.49207\ C_{L_u}$$

$$C_D = C_{D_u} + 0.00752\left(C_{L_u}\right)^2$$

$$C_m = C_{m_u} - 0.05110\ C_{L_u} \quad \text{(tail off)}$$

$$C_m = C_{m_u} - 0.05114\ C_{L_u} \quad \text{(tail on)}$$

It should be noted that corrections have not been applied for the effects of model support struts or for ram drag.

PRESENTATION OF DATA

Model configurations investigated in the wind-tunnel test are summarized in table 4. The basic model configuration was representative of a twin-engine commuter-transport aircraft except for the long wing-body fairing.

A summary of data given in figures 10 through 29 is given in table 5. Model component drag-buildup characteristics are presented in figure 10. The effects of flap deflection on the longitudinal aerodynamic characteristics of the model for two Reynolds numbers are presented in figure 11. Figure 12 presents the effects of Reynolds number on the longitudinal aerodynamic characteristics of the model for two flap deflections. The effects of Mach number on the longitudinal aerodynamic characteristics of the basic model configuration are presented in figure 13. The effects of placing transition strips on the surface of the basic model configuration are shown in figure 14. Figure 15 presents the effects of tail incidence on the longitudinal aerodynamic characteristics of the basic model configuration. The variation of side-force, yawing-moment, and rolling-moment coefficients with angle of sideslip for the basic model configuration are presented in figure 16.

The effects of tail incidence on the longitudinal aerodynamic characteristics for the low- and high-nacelle configurations are presented in figures 17 and 18, respectively. The effects of engine-nacelle position on the longitudinal aerodynamic characteristics of the model are presented in figure 19. Figure 20 presents the effects of Reynolds number on the longitudinal aerodynamic characteristics of the model with a partial-span drooped leading edge. A comparison of the longitudinal characteristics of the basic and partial-span drooped-leading-edge configurations for three Reynolds numbers is presented in figure 21. Pressure-distribution data for the two

TABLE 4.- MODEL CONFIGURATION SUMMARY

A-Basic configuration
1. Production wing leading edge
2. Production flap (double slotted)
3. Production tail
4. Production nacelles (mid-nacelles)
5. Long wing-body fairings

B-Partial-drooped-leading-edge configuration
Wing leading edge drooped outboard of nacelles

C-Drooped-leading-edge configuration
Wing leading edge has a full spanwise droop

D-High-nacelle configuration
High nacelles replace midnacelles in "A"

E-Low-nacelle configuration
Low nacelles replace midnacelles in "A"

F-Single-slotted-flap configuration
Single-slotted flap replaces production flap in "A"

G-Miscellaneous configurations
Wing-body
Wing-body-tail
Wing-body-tail-nacelles-gear
Wing-body-tail-nacelles-short-body fairings

spanwise locations of the wing-body configuration with and without the midwing nacelles are presented in figures 22 and 23. A comparison of the effects of tail incidence for the model with the double-slotted flap (basic flap configuration) and the model with the single-slotted flap is presented in figure 24. The basic (long) wing-body fairing is compared in figure 25 with the short wing-body fairing.

The model is normally mounted on the wind-tunnel support in an upright position. In order to evaluate flow-field effects arising from the strut mounting adapter, if any, the model was also tested in an inverted position. In figures 26 through 28 a comparison is made for several configurations. The effects of flap deflection on the longitudinal aerodynamic characteristics with full spanwise droop on the leading edge of the wing are presented in figure 29 (model inverted).

TABLE 5.- SUMMARY OF DATA FIGURES

Run no.	Figure	Mach no.	q		Reynolds number		α_u, deg	δ_f, deg	i_t, deg	ξ, deg	Remarks
			N/m^2	psf	$\times 10^6/m$	$\times 10^6/ft$					
5	10	0.210	11687.6	244.1	1.631	5.35	-4 to 4	---	---	0	Drag buildup
11		.210	12334.0	257.6	1.646	5.40	-4 to 14	0	---	↓	+ wing
13		.210	11792.9	246.3	1.640	5.38	-4 to 16	↓	0	↓	+ tail
16		.209	11826.4	247.0	1.631	5.35	-4 to 17	↓	↓	↓	+ nacelles
17		.211	11754.6	245.5	1.649	5.41	↓	↓	↓	↓	+ gear
46	11(a)	.159	6794.2	141.9	1.216	3.99	↓	0	↓	↓	Longitudinal data (basic configuration)
52		.157	6574.0	137.3	1.195	3.92	↓	18	↓	↓	
27		.160	6842.1	142.9	1.219	4.00	↓	36	↓	↓	
57		.160	6832.5	142.7	1.228	4.03	↓	54	↓	↓	
39	11(b)	.210	12386.6	258.7	1.649	5.41	↓	0	↓	↓	
52		.210	12108.9	252.9	1.634	5.36	-4 to 16	18	↓	↓	
19		.210	11965.3	249.9	1.634	5.36	-4 to 16	36	↓	↓	
46	12(a)	.159	6794.2	141.9	1.219	4.00	-4 to 17	0	↓	↓	Effect of Reynolds number (basic configuration)
39		.210	12386.6	258.7	1.649	5.41	-4 to 17	↓	↓	↓	
35		.263	18634.9	389.2	1.984	6.51	-4 to 15	↓	↓	↓	
32		.249	4227.8	88.3	.500	1.64	-4 to 17	↓	↓	↓	
27	12(b)	.160	6842.1	142.9	1.219	4.00	-4 to 17	36	↓	↓	
19		.210	11965.3	249.9	1.634	5.36	-4 to 16	↓	↓	↓	
31		.251	4294.9	89.9	.518	1.70	-4 to 17	↓	↓	↓	
39	13	.210	12386.6	258.7	1.649	5.41	-4 to 17	0	↓	↓	Effect of Mach number (basic configuration)
33		.338	19118.6	399.3	1.628	5.34	-4 to 14	↓	↓	↓	
39	14	.210	12386.6	258.7	1.649	5.41	-4 to 17	↓	↓	↓	Effect of transition (basic configuration)
20		.210	12075.4	252.2	1.631	5.35	-4 to 15	36	↓	↓	
144		.210	12065.8	252.0	1.631	5.35	-4 to 17	0	↓	↓	
147		.210	12185.5	254.5	1.631	5.35	-4 to 17	36	↓	↓	

TABLE 5.- CONTINUED

Run no.	Figure	Mach no.	q		Reynolds number		α_u, deg	δ_f, deg	i_t, deg	ℓ, deg	Remarks
			N/m^2	psf	$\times 10^6/m$	$\times 10^6/ft$					
43	15(a)	0.211	12343.5	257.8	1.655	5.43	0	0	-8 to +8	0	Effect of tail incidence (basic configuration)
44		.210	12233.4	255.5	1.649	5.41	4	↓	↓	↓	↓
45		.210	12123.3	253.2	1.640	5.38	8	↓	↓	↓	↓
53	15(b)	.158	6597.9	137.8	1.198	3.93	0	18	↓	↓	↓
54		.160	6737.7	140.7	1.213	3.98	4	↓	↓	↓	↓
55		.160	6703.2	140.0	1.213	3.98	8	↓	↓	↓	↓
24	15(c)	.210	11903.0	248.6	1.625	5.33	0	36	↓	↓	↓
25		.210	11931.8	249.2	1.625	5.33	4	↓	↓	↓	↓
26		.210	11926.9	249.1	1.622	5.32	8	↓	↓	↓	↓
40	16(a)	.210	12266.9	256.2	1.646	5.40	0	0	0	-2 to +6	Lateral-directional data (basic configuration)
41		.210	12310.0	251.1	1.649	5.41	4	↓	↓	↓	↓
42		.209	12180.7	254.4	1.643	5.39	8	↓	↓	↓	↓
21	16(b)	.209	11874.3	248.0	1.628	5.34	0	36	↓	↓	↓
22		.210	11926.9	249.1	1.628	5.34	4	↓	↓	↓	↓
23		.208	11773.8	245.9	1.618	5.31	8	↓	↓	↓	↓
100	17(a)	.210	11725.9	244.9	1.622	5.32	0	0	-8 to +8	0	Tail incidence (low nacelle)
101		.209	11673.2	243.8	1.615	5.30	4	↓	↓	↓	↓
102		.209	11706.7	244.5	1.612	5.29	8	↓	↓	↓	↓
116	17(b)	.209	11831.2	247.1	1.628	5.34	0	36	↓	↓	↓
117		.210	11950.9	249.6	1.631	5.35	4	↓	↓	↓	↓
118		.210	11941.3	249.4	1.628	5.34	8	↓	↓	↓	↓
74	18(a)	.210	11864.7	247.8	1.634	5.36	0	0	↓	↓	Tail incidence (high nacelle)
75		.210	11845.6	247.4	1.631	5.35	4	↓	↓	↓	↓
76		.210	11826.4	247.0	1.628	5.34	8	↓	↓	↓	↓

TABLE 5.- CONTINUED

Run no.	Figure	Mach no.	q		Reynolds number		α_u, deg	δ_f, deg	i_t, deg	β, deg	Remarks
			N/m^2	psf	$\times 10^6/m$	$\times 10^6/ft$					
90	18(b)	0.211	12008.4	250.8	1.640	5.38	0	36	-8 to +8	0	Tail incidence (high nacelle)
91		.210	11864.7	247.8	1.628	5.34	4	↓			
92		.210	11869.5	247.9	1.625	5.33	8				
13	19	.210	11792.9	246.3	1.640	5.38	-4 to 16	0	0		Effect of nacelle location
39		.210	12386.6	258.7	1.649	5.41	-4 to 17				
73		.210	11888.7	248.3	1.637	5.37	-4 to 16				
99		.209	11692.4	244.2	1.625	5.33	-4 to 16				
60	20	.160	6693.7	139.8	1.219	4.008	-4 to 17				Effect of Reynolds number (partial-drooped leading edge)
65		.210	11917.4	248.9	1.663	5.456	-4 to 16				
64		.298	21919.6	457.8	2.105	6.91	-4 to 15				
46	21	.159	6794.2	141.9	1.216	3.99	-4 to 17				Basic leading edge configuration, partial-span drooped leading edge, basic leading edge, partial-drooped leading edge
60		.160	6693.7	139.8	1.219	4.01	↓				
57		.160	6832.5	142.7	1.228	4.03		54			
59		.159	6660.1	139.1	1.219	4.00		54			
123	22(a)	.209	11567.9	241.6	1.628	5.34	0,4,8,12, 16	0			Wing-body pressures (outboard strap)
123	22(b)	.209	11567.9	241.6	1.628	5.34					(inboard strap)
126	23(a)	.208	11740.2	245.2	1.618	5.31					Wing-body mid-nacelles (outboard strap)
126	23(b)	.208	11740.2	245.2	1.618	5.31	↓	↓	↓	↓	(inboard strap)

TABLE 5.- CONCLUDED

Run no.	Figure	Mach no.	q		Reynolds number		α_u, deg	δ_f, deg	i_t, deg	3, deg	Remarks
			N/m^2	psf	$\times 10^6/m$	$\times 10^6/ft$					
25	24	0.210	11931.8	249.2	1.625	5.33	4	36	-8 to	0	Tail effectiveness (single- and double-slotted flap)
138		.208	11831.2	247.1	1.609	5.28	4	36	+8		
39	25(a)	.210	12386.6	258.7	1.649	5.41	-4 to 17	0	0		Short and long wing-body fairing with and without transition
153		.210	12118.5	253.1	1.646	5.40					
144		.210	12065.8	252.0	1.631	5.35					
151		.210	12003.6	250.7	1.631	5.35					
32	25(b)	.249	4227.8	88.3	.500	1.64					Short and long wing-body fairing with and without transition
154		.249	4237.4	88.5	.521	1.71					
146		.251	4275.7	89.3	.512	1.68					
152		.249	4218.3	88.1	.518	1.70					
11	26(a)	.210	12334.0	257.6	1.646	5.40	-4 to 14				Comparison of model mounting
169		.210	11979.6	250.2	1.646	5.40	-4 to 10				
134	26(b)	.209	11821.6	246.9	1.625	5.33	-4 to 17	36			
172		.210	11998.8	250.6	1.637	5.37	-4 to 10	36			
129	27	.210	11826.4	247.0	1.631	5.35	-4 to 17	0			Comparison of midwing and high nacelle, model upright, model inverted
132		.211	12041.9	251.5	1.640	5.38	-4 to 17				
176		.210	11883.9	248.2	1.628	5.34	-4 to 10				
177		.210	11907.8	248.7	1.634	5.36	-4 to 10				
9	28	.298	21723.2	453.7	2.131	6.99	-4 to 16	---	---		Comparison of inverted and upright (fuselage only)
179		.299	22451.1	468.9	2.131	6.99	-4 to 10	---	---		
163	29	.209	12017.9	251.0	1.628	5.34		0	0		Model inverted, full drooped leading edge
157		.210	11994.0	250.5	1.634	5.36		18			
160		.211	11864.7	247.8	1.652	5.42		36			
162		.211	11998.8	250.6	1.628	5.34		54			

DATA DOCUMENTATION

Only a portion of the data recorded during the test program is presented in the figures of this report. For completeness, all the wind-tunnel test data are included in Appendix A.

APPENDIX A

TABULATED TEST DATA

Since only a portion of the wind-tunnel test data is presented in plotted form in this report, all the test data are presented on microfiche in the attached jackets. Coded configuration designations used during the wind-tunnel test are shown in table 1A. A tabulation of the model configuration tested is presented in table 2A. The aerodynamic coefficients used on the microfiche records are defined in table 3A, and a quick reference to the available data is presented in table 4A.

TABLE 1A.- CODED CONFIGURATION DESIGNATION FOR TEST

Basic configuration	Code
Production fuselage	B
Production wing leading edge	W1
Production flap (double slotted)	F1
Production tail	T1
Production nacelles (midnacelles)	N1
Other configurations	
Drooped-wing leading edge (outboard of nacelles)	W2
High nacelles	N2
Low nacelles	N3
Pressure straps	PS
Single-slotted flap	F2
Landing gear	G

TABLE 2A.- SUMMARY OF WIND-TUNNEL TEST CONFIGURATIONS

Test configuration	Production-wing leading edge	Double-slotted flap	Mid-nacelles	High nacelles	Low nacelles	Landing gear	Tail	Drooped-wing leading edge	Drooped-wing leading edge outboard	Single-slotted flap
Basic configuration	✓	✓	✓				✓			
Drooped-wing leading edge	✓	✓	✓				✓		✓	
High nacelles	✓	✓		✓			✓			
Low nacelles	✓	✓			✓		✓			
Wing pressure	✓	✓								
Wing pressure	✓	✓	✓							
Flow visualization	✓	✓	✓							
Flow visualization	✓	✓		✓						
Flow visualization	✓	✓								
Single-slotted flap	✓		✓				✓			✓
With transition	✓	✓	✓				✓			
Short-body fairing with transition	✓	✓	✓				✓			
Short-body fairing	✓	✓	✓				✓			
Model inverted	✓	✓	✓							
Inverted with gear	✓	✓	✓			✓				
Inverted with drooped leading edge	✓	✓	✓					✓		
Inverted, no nacelles	✓	✓						✓		
Inverted, mid-nacelles	✓	✓	✓							
Inverted, high nacelles	✓	✓		✓						
Inverted, low nacelles	✓	✓			✓					

TABLE 3A.- MICROFICHE AERODYNAMIC SYMBOLS

CL	Lift coefficient
CD	Drag coefficient
CM	Pitching-moment coefficient
CY	Side-force coefficient
CYM	Yawing-moment coefficient
CRM	Rolling-moment coefficient
CA	Axial-force coefficient
CN	Normal-force coefficient

TABLE 4A.- TEST RUN SUMMARY

Conversion factors:

ft × 0.3048 = m

psf × 47.880258 = N/m^2

psi × 6894.7572 = N/m^2

Run no.	p_0, psi	q, psf	Reynolds number, $\times 10^6$/ft	α_u, deg	δ_f, deg	i_t, deg	β, deg	Mach no.	Remarks
1	---	---	---	---	---	---	---	---	Calibration check, 2.5-in. balance
2	---	---	---	---	---	---	---	---	Calibration check, 2.5-in. balance
3	14.7	89.1	1.709	-4 to 4	---	---	0	0.250	Configuration B
4	60.0	138.4	4.001	↓	---	---	↓	.159	↓
5	↓	244.1	5.349	↓	---	---	↓	.210	↓
6	↓	473.5	6.981	↓	---	---	↓	.299	↓
7,8	---	---	---	---	---	---	---	---	Calibration check, 4-in. balance
9	60.0	453.7	6.978	-4 to 16	---	---	0	.298	Configuration B
10	↓	464.4	6.998	-4 to 11	0	---	↓	.300	Configuration B + W1[a]
11	↓	257.6	5.400	-4 to 14	↓	---	↓	.210	Configuration B + W1[a]
12	↓	142.2	3.988	-4 to 17	↓	---	↓	.160	Configuration B + W1[a]
13	↓	246.3	5.378	-4 to 16	↓	0	↓	.210	Configuration B + W1 + T1[b]
14	↓	142.3	4.046	-4 to 17	↓	↓	↓	.161	↓
15	↓	461.3	6.927	-4 to 13	↓	↓	↓	.300	↓
16	↓	247.0	5.354	-4 to 17	↓	↓	↓	.209	Configuration B + W1 + T1 + N1[c]
17	↓	245.5	5.408	↓	↓	↓	↓	.211	Configuration B + W1 + T1 + N1 + G[d]
18	↓	249.4	5.372	↓	36	↓	↓	.210	Configuration B+W1+F1+T1+N1+G
19	↓	249.9	5.363	-4 to 15	↓	↓	↓	.210	Configuration B+W1+F1+T1+N1
20	↓	252.2	5.354	-4 to 16	↓	↓	↓	.210	Configuration B+W1+F1+T1+N1 and strut fairing
21	↓	248.0	5.335	0	↓	↓	-2 to 6	.210	Configuration B+W1, F1, T1, N1 (basic configuration)
22	↓	249.1	5.341	4	↓	↓	↓	.210	↓
23	↓	245.9	5.305	8	↓	↓	↓	.208	↓
24	↓	248.6	5.332	0	↓	-4 to 8	0	.210	↓
25	↓	249.2	5.331	4	↓	↓	↓	.210	↓
26	↓	249.1	5.322	8	↓	↓	↓	.210	↓
27	↓	142.9	4.001	-4 to 17	↓	0	↓	.160	↓

TABLE 4A.- CONTINUED

Run no.	p_0, psi	q, psf	Reynolds number, $\times 10^6$/ft	α_u, deg	δ_f, deg	i_t, deg	β, deg	Mach no.	Remarks
28	60.0	142.9	3.994	0	36	-4 to 8	0	0.160	Configuration B + W1, F1, T1, N1 (basic configuration)
29	↓	141.7	3.987	4	↓	↓	↓	.160	↓
30	↓	141.3	3.980	8	↓	↓	↓	.160	↓
31	14.7	89.7	1.701	-4 to 17	↓	0	↓	.251	↓
32	14.7	88.3	1.642	-4 to 17	0	↓	↓	.249	↓
33	40.0	413.1	5.413	-4 to 14	↓	↓	↓	.345	↓
34	60.0	465.0	6.998	-4 to 15	↓	↓	↓	.301	↓
35	↓	389.2	6.506	-4 to 15	↓	↓	↓	.263	↓
36	↓	386.7	6.490	0	↓	-8 to 8	↓	.262	↓
37	↓	385.6	6.471	4	↓	↓	↓	.262	↓
38	↓	379.9	6.411	8	↓	↓	↓	.260	↓
39	↓	259.7	5.409	-4 to 17	↓	0	↓	.210	↓
40	↓	256.2	5.400	0	↓	↓	-2 to 6	.210	↓
41	↓	257.1	5.415	4	↓	↓	↓	.210	↓
42	↓	254.4	5.389	8	↓	↓	↓	.210	↓
43	↓	257.8	5.428	0	↓	-8 to 8	0	.210	↓
44	↓	255.5	5.406	4	↓	↓	↓	.210	↓
45	↓	253.2	5.382	8	↓	↓	↓	.210	↓
46	↓	141.9	3.994	-4 to 17	↓	0	↓	.159	↓
47	↓	140.7	3.997	0	↓	-8 to 8	↓	.159	↓
48	↓	142.6	4.018	4	↓	↓	↓	.161	↓
49	↓	140.7	3.997	8	↓	↓	↓	.160	↓
50	↓	372.1	6.463	-4 to 16	18	0	↓	.200	↓
51	↓	252.9	5.355	-4 to 16	↓	↓	↓	.210	↓
52	↓	137.3	3.915	-4 to 17	↓	↓	↓	.157	↓
53	↓	137.8	3.934	0	↓	-8 to 8	↓	.158	↓
54	↓	140.7	3.982	4	↓	↓	↓	.160	↓
55	↓	140.0	3.977	8	↓	↓	↓	.160	↓
56	14.7	90.7	1.740	-4 to 17	↓	0	↓	.253	↓
57	60.0	142.7	4.026	↓	54	↓	↓	.160	↓
58	14.7	90.2	1.737	↓	54	↓	↓	.252	↓

TABLE 4A.- CONTINUED

Run no.	p_0, psi	q, psf	Reynolds number, $\cdot 10^6$/ft	α_u, deg	δ_f, deg	i_t, deg	β, deg	Mach no.	Remarks
59	60.0	139.1	3.996	-4 to 17	54	0	0	0.159	Configuration B + W2, F1, T1, N1 partial-droop leading edge, outboard nacelles
60		139.8	4.008	-4 to 17	0	0		.160	
61		139.0	3.995	0		-8 to 8		.160	
62		138.1	3.982	4				.160	
63		138.3	3.982	8				.160	
64		457.8	6.910	-4 to 17		0		.298	
65		248.9	5.456	-4 to 16		0		.210	
66		250.7	5.429	0		-8 to 8		.212	
67		247.4	5.368	4				.211	
68		245.8	5.334	8				.210	
69		370.2	6.430	-4 to 14		0		.260	
70		373.6	6.390	0		-8 to 8		.260	
71		373.1	6.374	4				.260	
72		373.2	6.360	8				.260	
73		248.3	5.371	-4 to 16		0		.210	Configuration B + W1, F1, T1, N2
74		247.8	5.356	0		-8 to 8		.210	
75		247.4	5.345	4				.210	
76		247.0	5.336	8				.210	
77		367.0	6.405	0				.259	
78		371.5	6.403	4				.260	
79		366.9	6.337	8				.258	
80		369.1	6.335	-4 to 14		0		.259	
81		144.0	4.001	-4 to 17		0		.159	
82		144.7	4.036	0		-8 to 8		.161	
83		143.2	4.025	4				.160	
84		141.5	4.005	8				.159	
85		467.6	6.979	-4 to 14		0		.300	
86		247.2	5.331	-4 to 16	18			.209	
87		368.7	6.425	-2 to 14				.209	
88		141.0	3.955	-4 to 17				.160	

TABLE 4A.- CONTINUED

Run no.	p_o, psi	q, psf	Reynolds number, $\times 10^6$/ft	α_u, deg	δ_f, deg	i_t, deg	β, deg	Mach no.	Remarks
89	60.0	248.6	5.367	-4 to 16	36	0	0	0.210	Configuration B + W1, F1, T1, N2
90	↓	250.8	5.378	0	↓	-8 to 8	↓	.211	↓
91	↓	247.7	5.340	4	↓	↓	↓	.210	↓
92	↓	247.9	5.328	8	↓	↓	↓	.210	↓
93	↓	142.1	4.014	-4 to 17	↓	0	↓	.160	↓
94	↓	141.8	4.010	0	↓	-8 to 8	↓	.160	↓
95	↓	140.6	3.994	4	↓	↓	↓	.159	↓
96	↓	141.4	4.003	8	↓	↓	↓	.160	↓
97	↓	145.1	4.076	-4 to 15	54	0	↓	.161	↓
98	↓	140.5	4.022	-4 to 15	54	↓	↓	.160	Configuration B + W1, F1, T1, N3
99	↓	244.2	5.330	-4 to 16	0	↓	↓	.209	↓
100	↓	244.9	5.319	0	↓	-8 to 8	↓	.210	↓
101	↓	243.8	5.296	4	↓	↓	↓	.209	↓
102	↓	244.5	5.290	8	↓	↓	↓	.209	↓
103	↓	370.7	6.427	-4 to 14	↓	0	↓	.260	↓
104	↓	370.6	6.385	0	↓	-8 to 8	↓	.259	↓
105	↓	371.6	6.373	4	↓	↓	↓	.259	↓
106	↓	370.5	6.347	8	↓	↓	↓	.259	↓
107	↓	137.0	3.988	-4 to 17	↓	0	↓	.160	↓
108	↓	137.5	3.985	0	↓	-8 to 8	↓	.160	↓
109	↓	137.4	3.979	4	↓	↓	↓	.160	↓
110	↓	136.5	3.962	8	↓	↓	↓	.159	↓
111	↓	459.2	6.978	-4 to 14	↓	0	↓	.300	↓
112	↓	246.9	5.378	-4 to 16	18	↓	↓	.210	↓
113	↓	370.4	6.469	-4 to 14	↓	↓	↓	.260	↓
114	↓	144.3	4.018	-4 to 17	↓	↓	↓	.161	↓
115	↓	249.7	5.384	-4 to 13	36	↓	↓	.210	↓
116	↓	247.1	5.338	0	↓	-8 to 8	↓	.209	↓
117	↓	249.6	5.350	4	↓	↓	↓	.210	↓
118	↓	249.4	5.337	8	↓	↓	↓	.210	↓
119	↓	144.4	4.046	0	↓	↓	↓	.161	↓
120	↓	142.3	4.021	4	↓	↓	↓	.160	↓

TABLE 4A.- CONTINUED

Run no.	p_0, psi	q, psf	Reynolds number, $\times 10^6$/ft	α_u, deg	δ_f, deg	i_t, deg	β, deg	Mach no.	Remarks
121	60.0	141.6	4.009	8	36	-8 to 8	0	0.160	Configuration B + W1, F1, T1, N3
122	↓	143.0	4.027	-4 to 17	36	0	↓	.161	Configuration B + W1, F1, T1, N3
123	↓	244.0	5.336	↓	0	↓	↓	.209	Configuration B + W1, F1, pressure straps
124	↓	139.2	4.000	↓	↓	↓	↓	.159	↓
125	14.7	90.0	1.724	↓	↓	↓	↓	.251	↓
126	60.0	245.2	5.308	↓	↓	↓	↓	.208	Configuration B + W1, F1, N1, pressure straps
127	60.0	142.9	4.033	↓	↓	↓	↓	.161	↓
128	14.7	88.6	1.715	↓	↓	↓	↓	.249	↓
129	60.0	247.1	5.355	-4 to 16	↓	↓	↓	.210	Configuration B + W1, F1, N1, flow visualization
130	↓	244.7	5.325	↓	36	↓	↓	.210	Configuration B + W1, F1, N1, flow visualization
131	↓	248.8	5.360	↓	36	↓	↓	.210	Configuration B + W1, F1, N2, flow visualization
132	↓	251.5	5.378	↓	0	↓	↓	.211	Configuration B + W1, F1, N2, flow visualization
133	↓	248.6	5.335	↓	0	↓	↓	.210	Configuration B + W1, F1, flow visualization
134	↓	246.9	5.330	↓	36	↓	↓	.209	Configuration B + W1, F1, flow visualization
135	↓	137.9	3.990	-4 to 17	54	↓	↓	.159	Configuration B + W1, F2, T1, N1
136	↓	249.1	5.346	-4 to 17	36	↓	↓	.210	↓
137	↓	244.9	5.277	0	↓	-8 to 8	↓	.208	↓
138	↓	247.1	5.283	4	↓	↓	↓	.208	↓
139	↓	246.8	5.263	8	↓	↓	↓	.208	↓
140	↓	143.2	3.982	-4 to 17	↓	0	↓	.159	↓
141	↓	144.8	3.999	0	↓	-8 to 8	↓	.160	↓
142	↓	145.0	3.998	4	↓	↓	↓	.160	↓
143	↓	143.9	3.978	8	↓	↓	↓	.160	↓
144	↓	252.0	5.346	-4 to 17	0	0	↓	.210	Configuration B + W1, F1, T1, N1, with transition

TABLE 4A.- CONTINUED

Run no.	p_0, psi	q, psf	Reynolds number, $\times 10^6$/ft	α_u, deg	δ_f, deg	i_t, deg	β, deg	Mach no.	Remarks
145	60.0	468.1	6.937	-4 to 16	0	0	0	0.299	Configuration B + W1, F1, T1, N1, with transition
146	14.7	89.3	1.676	-4 to 17	0			.251	
147	60.0	254.5	5.350		36			.210	
148	14.7	89.7	1.707					.251	
149	60.0	250.6	5.378					.210	Configuration B + W1, F1, T1, N1, with transition, with short wing-body fairing
150	14.7	89.1	1.716					.250	
151	60.0	250.7	5.350		0			.210	
152	14.7	88.1	1.703					.249	
153	60.0	253.1	5.398					.210	Configuration B + W1, F1, T1, N1, (transition removed) with short wing-body fairing
154	14.7	88.5	1.707					.249	Configuration B + W1, F1, T1, N1, (transition removed) with short wing-body fairing
155[e]	60.0	246.3	5.339	-4 to 10	18			.209	Configuration B + W1, F1, N1, model inverted
156		252.1	5.381					.211	Configuration B + W1, F1, N1, G
157		250.5	5.363					.210	Configuration B + W2, F1, N1, full-spanwise-drooped leading edge
158		369.4	6.459					.260	
159		141.5	4.000					.160	
160		247.8	5.417		36			.211	
161		140.8	4.030		36			.160	
162		250.6	5.336		54			.211	
163		251.0	5.337		0			.209	
164		367.0	6.379					.257	
165		143.8	3.986					.160	
166		250.9	5.329					.209	Configuration B + W2, F1, full-spanwise-drooped leading edge

TABLE 4A.- CONCLUDED

Run no.	p_0, psi	q, psf	Reynolds number, $\times 10^6$/ft	α_u, deg	δ_f, deg	i_t, deg	β, deg	Mach no.	Remarks
167	60.0	371.3	6.388	-4 to 10	0	0	0	0.259	Configuration B + W2, F1, full-spanwise-drooped leading edge
168		141.1	3.931					.159	Configuration B + W2, F1, full-spanwise-drooped leading edge
169		250.1	5.397					.210	Configuration B + W1, F1, full-spanwise-dropped leading edge
170		458.8	7.005					.298	
171		146.2	4.029					.161	
172		250.6	5.368		36			.210	
173		147.1	4.017					.160	
174		249.4	5.351					.210	Configuration B + W1, F1, N1, sting body top of strut
175		248.3	5.374					.210	Configuration B + W1, F1, N1
176		248.1	5.340		0			.210	Configuration B + W1, F1, N1
177		248.6	5.361					.210	Configuration B + W1, F1, N2
178		247.9	5.404					.211	Configuration B + W1, F1, N3
179		468.9	6.992		---	---	---	.299	Configuration B

[a] Wing

[b] Tail

[c] Nacelle

[d] Landing gear

[e] Model mounted inverted Run no. 155 through 179.

REFERENCES

1. Brusse, J. C.; and Ribbe, J. H.: Wind Tunnel Test of the Merlin III for Swearingen Aviation Corporation. Texas Eng. Exp. Station, Texas A&M Univ., Oct. 1978.

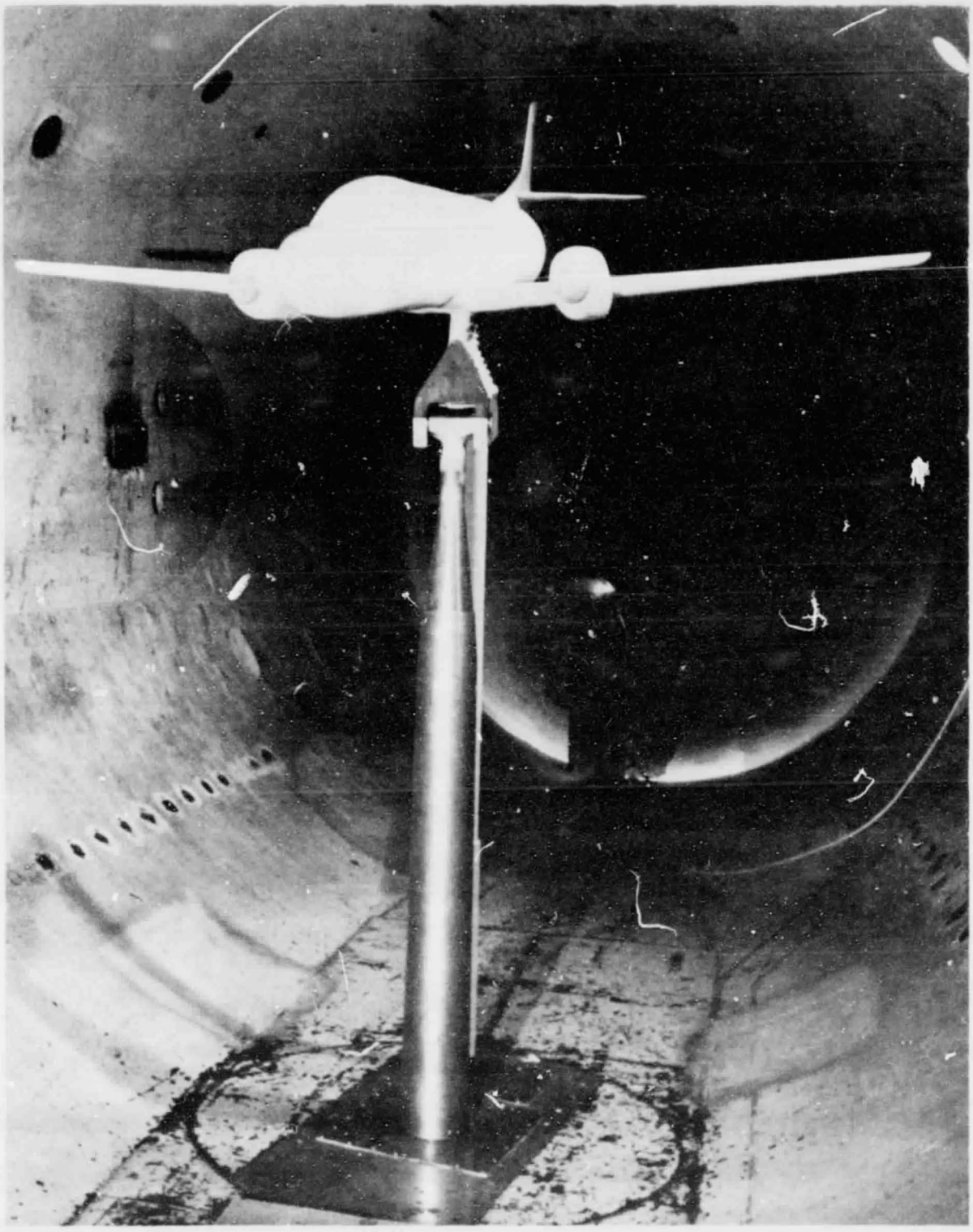

Figure 1.- Photograph of basic model mounted in Ames 12-Foot Pressure Wind Tunnel.

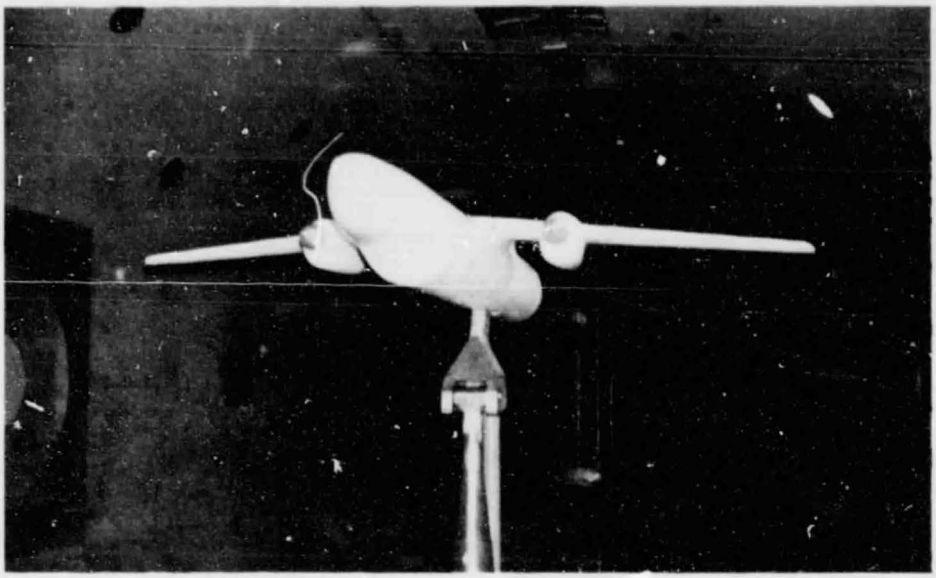

Figure 2.- Three-quarter front view of model mounted inverted.

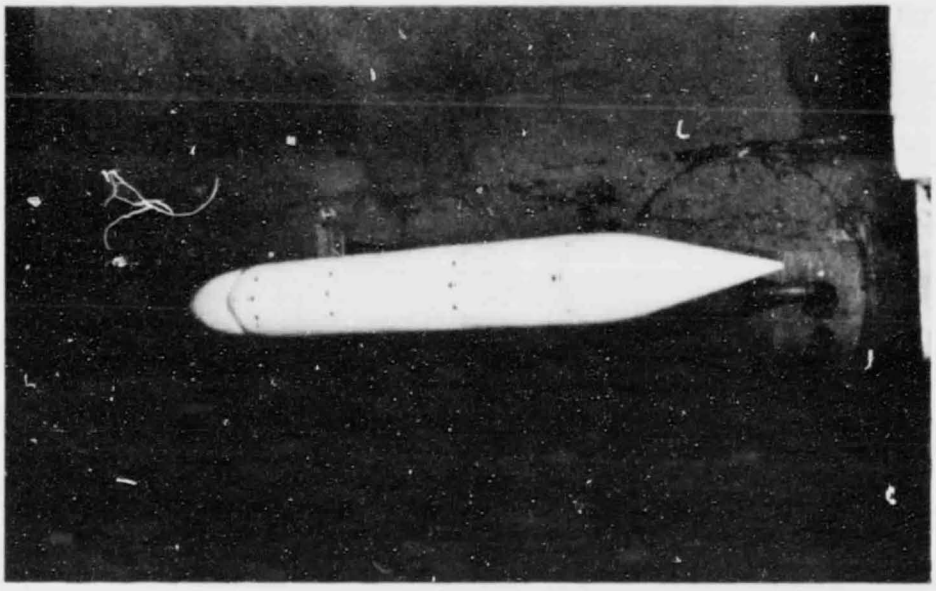

Figure 3.- Top view of fuselage-only configuration.

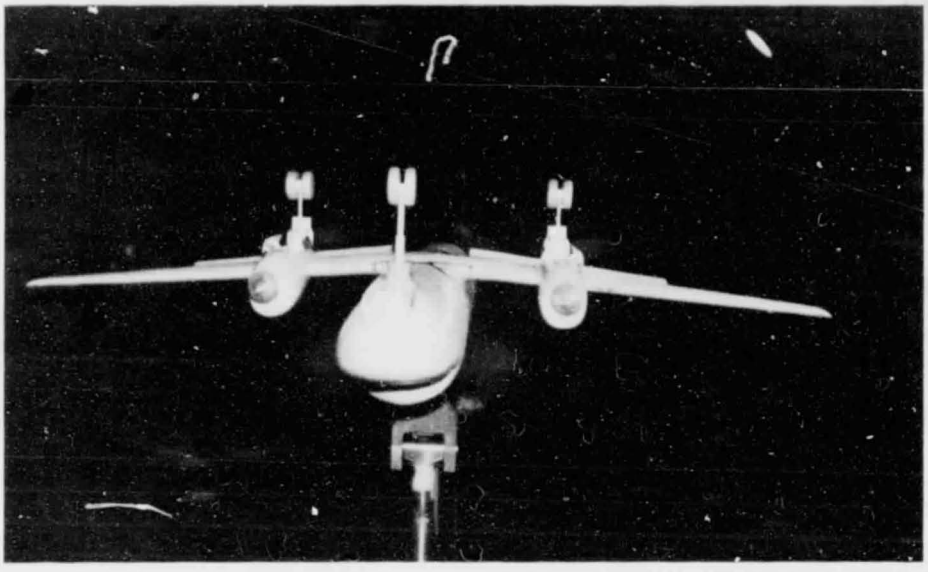

Figure 4.- Photograph of model with landing gear; model mounted inverted.

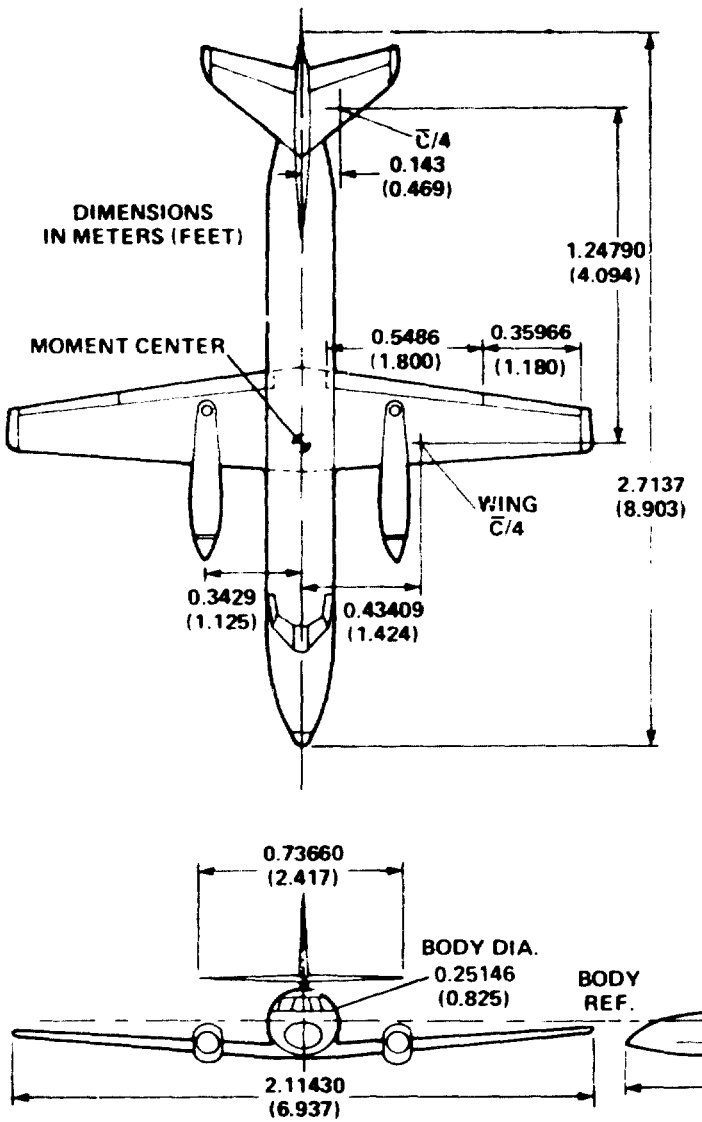

		WING	HORIZONTAL TAIL	VERTICAL TAIL
AREA,	m^2	0.57971	0.15143	0.08826
	ft^2	(6.240)	(1.630)	(0.950)
ASPECT RATIO		7.71	3.58	2.11
TAPER RATIO		0.398	0.463	0.445
b,	m	2.11430	0.73660	0.43180
	ft	(6.937)	(2.417)	(1.417)
C_{ROOT},	m	0.39268	0.30480	0.31750
	ft	(1.288)	(1.00)	(1.042)
C_{TIP},	m	0.15646	0.14122	0.14122
	ft	(0.513)	(0.463)	(0.463)
C̄,	m	0.29134	0.24257	0.24638
	ft	(0.956)	(0.796)	(0.808)
L.E. SWEEP		4.5°	39°	39°
T.E. SWEEP		-9.0°	15.5°	15.5°
AIRFOIL SECTION				
ROOT		65_2A215	66A009	66A009
TIP		64_2A415	63A009	63A009

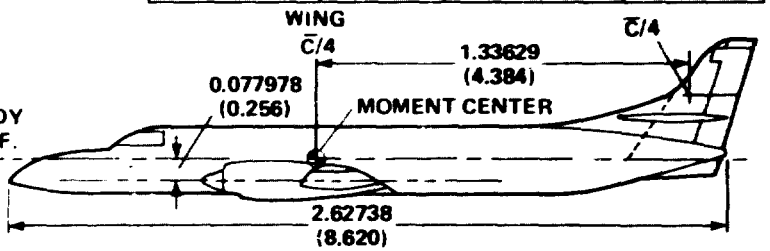

Figure 5.- Geometric details of model.

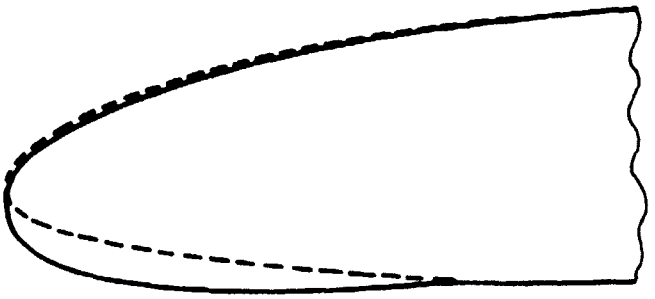

—— DROOPED L.E.
--- BASIC L.E.

MODEL LEADING EDGE DETAIL

UPPER SURFACE		LOWER SURFACE	
X/C	Y/C	X/C	Y/C
0.000000	-0.009950	0.000000	-0.009950
0.000995	-0.002587	0.000199	-0.013632
0.001990	0.000398	0.000398	-0.015025
0.002985	0.002687	0.000597	-0.016020
0.003980	0.004577	0.000995	-0.017612
0.005970	0.007761	0.001990	-0.020299
0.007960	0.010448	0.002985	-0.022289
0.010945	0.013731	0.003980	-0.023980
0.012935	0.015622	0.009950	-0.030448
0.015323	0.017711	0.019900	-0.036816
0.028258	0.025871	0.029851	-0.040896
0.038109	0.030249	0.039800	-0.043980
0.067861	0.040896	0.069652	-0.049552
0.097612	0.049751	0.099502	-0.052239
0.162388	0.064179	0.174129	-0.054328
0.242285	0.076219	0.248756	-0.056219

(a) Drooped-wing-leading-edge configuration.

Figure 6.- Alternate-configuration geometry.

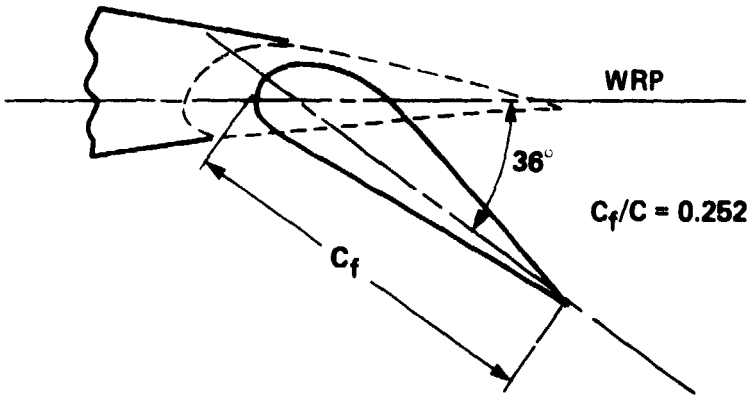

ALTERNATE CONFIGURATION

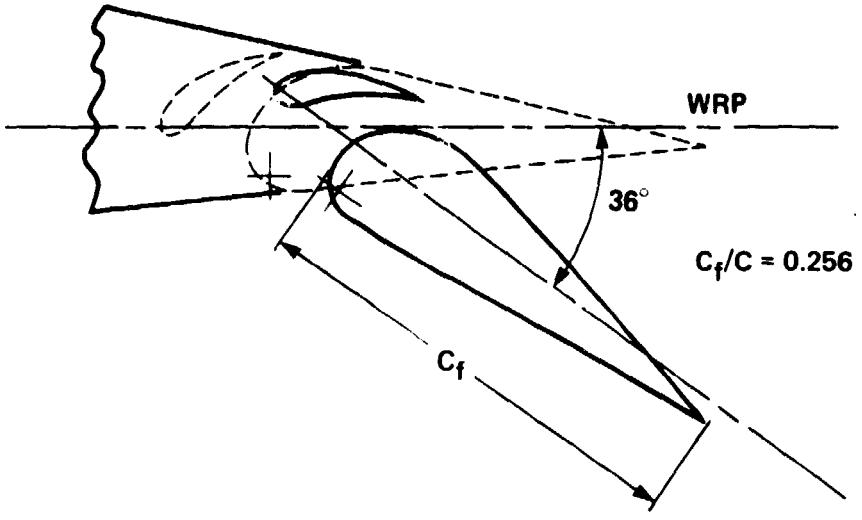

BASIC CONFIGURATION

(b) Details of model flap configurations.

Figure 6.- Continued.

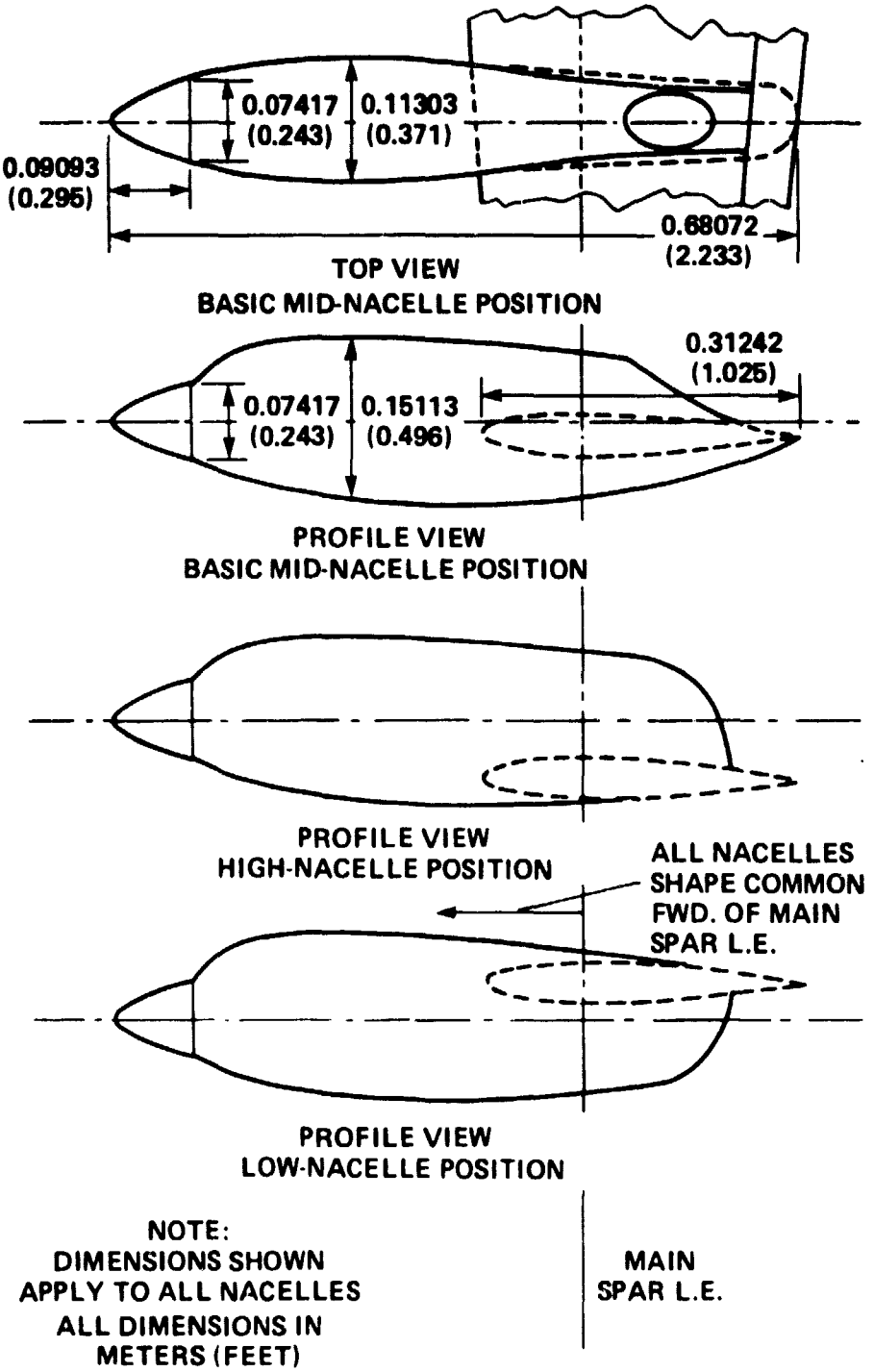

(c) Details of nacelle configurations.

Figure 6.- Concluded.

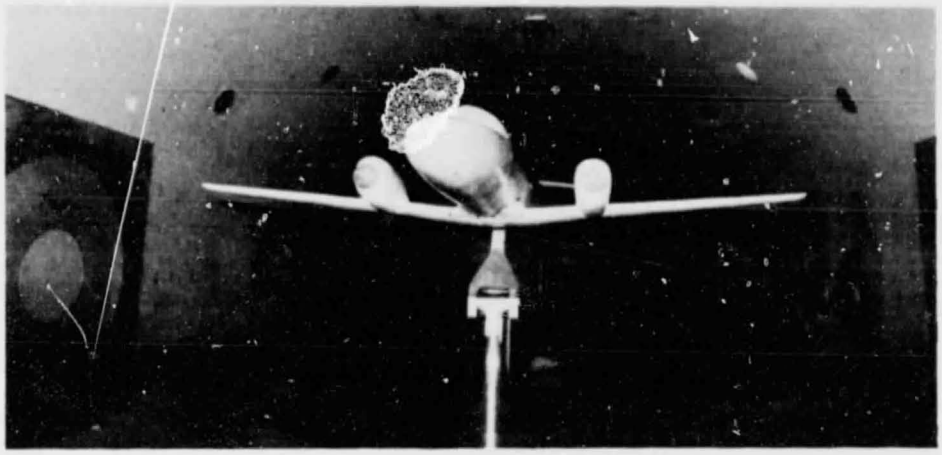

(a) High nacelle.

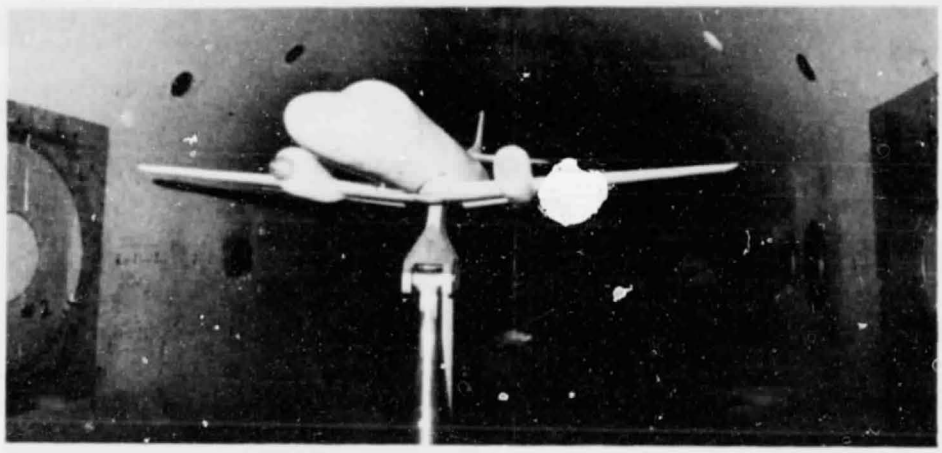

(b) Midnacelle.

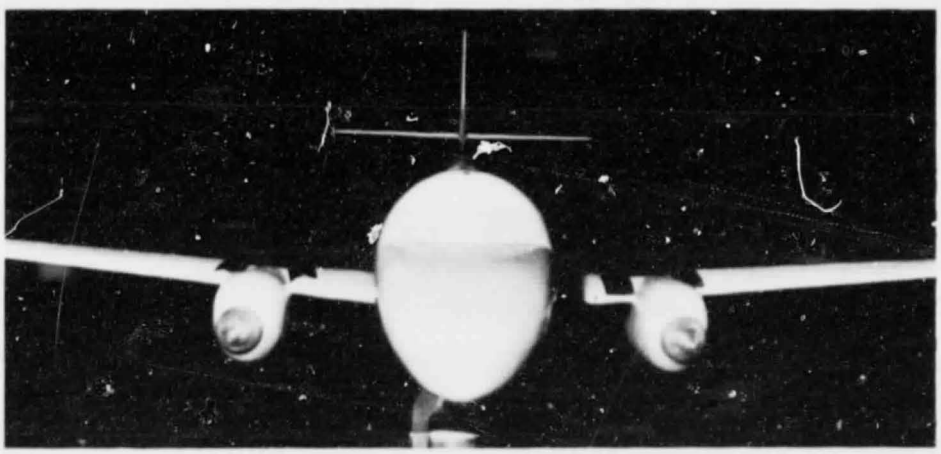

(c) Low nacelle.

Figure 7.- Photographs showing nacelle locations investigated.

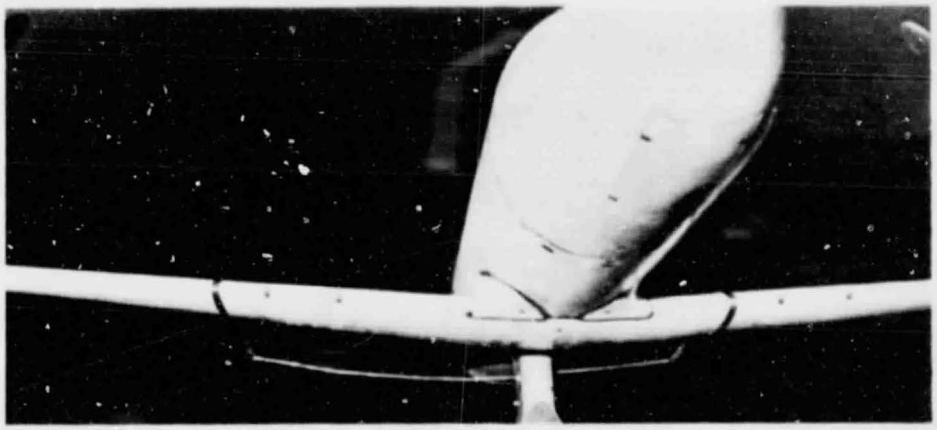

(a) Plain wing.

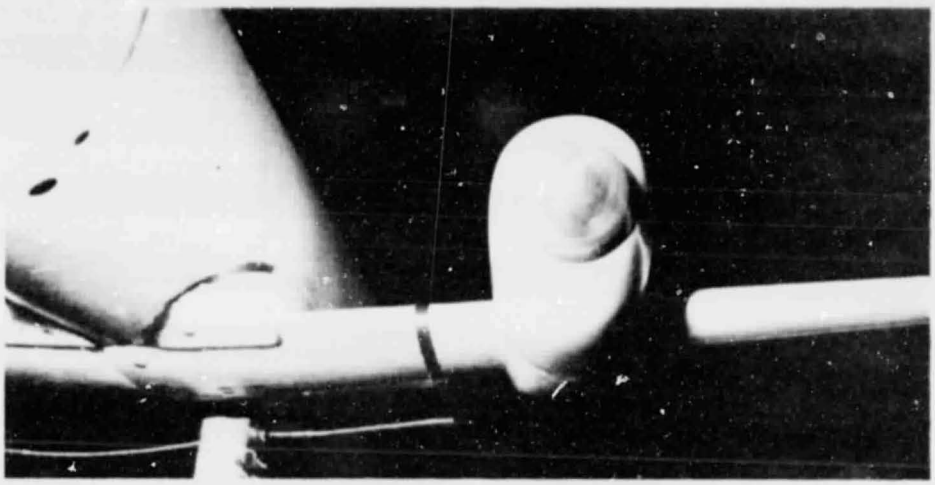

(b) Pressure-strap detail with left nacelle installed.

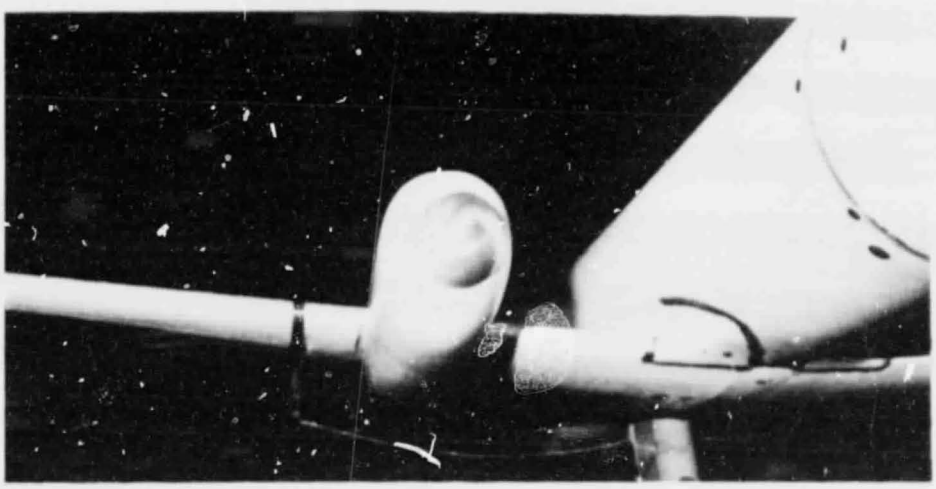

(c) Pressure-strap detail with right nacelle installed.

Figure 8.- Photographs of pressure straps mounted on modal.

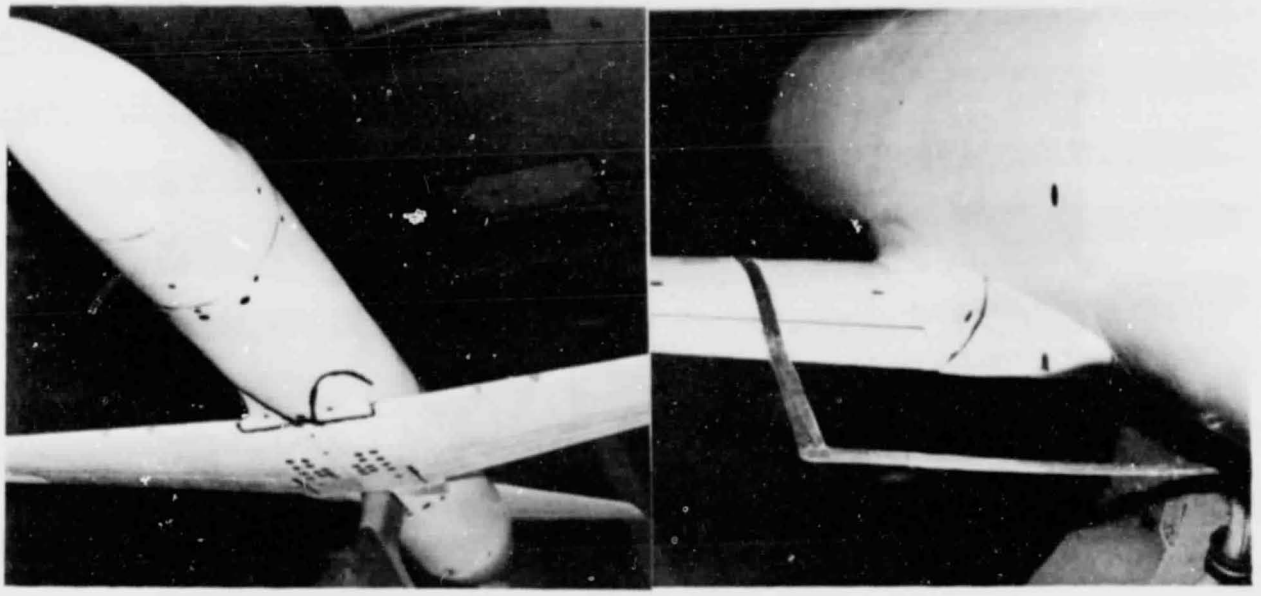

Front view Rear view

(a) Long wing-body fairing (basic configuration).

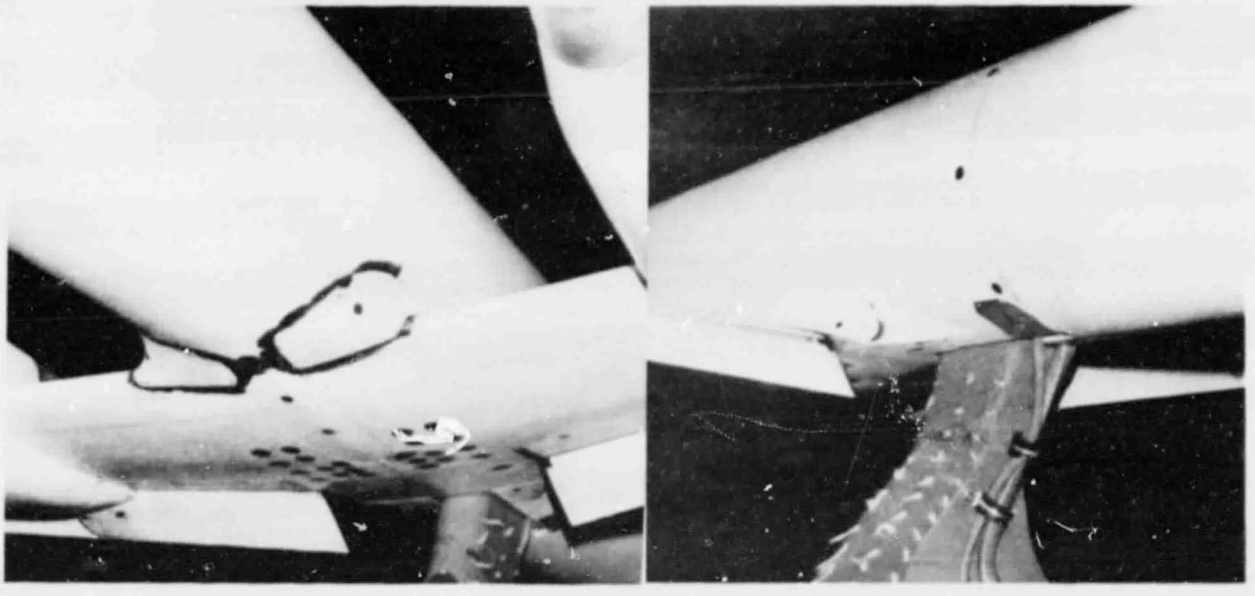

Front view Rear view

(b) Short wing-body fairing.

Figure 9.- Photographs of wing-body fairings used in wind-tunnel test.

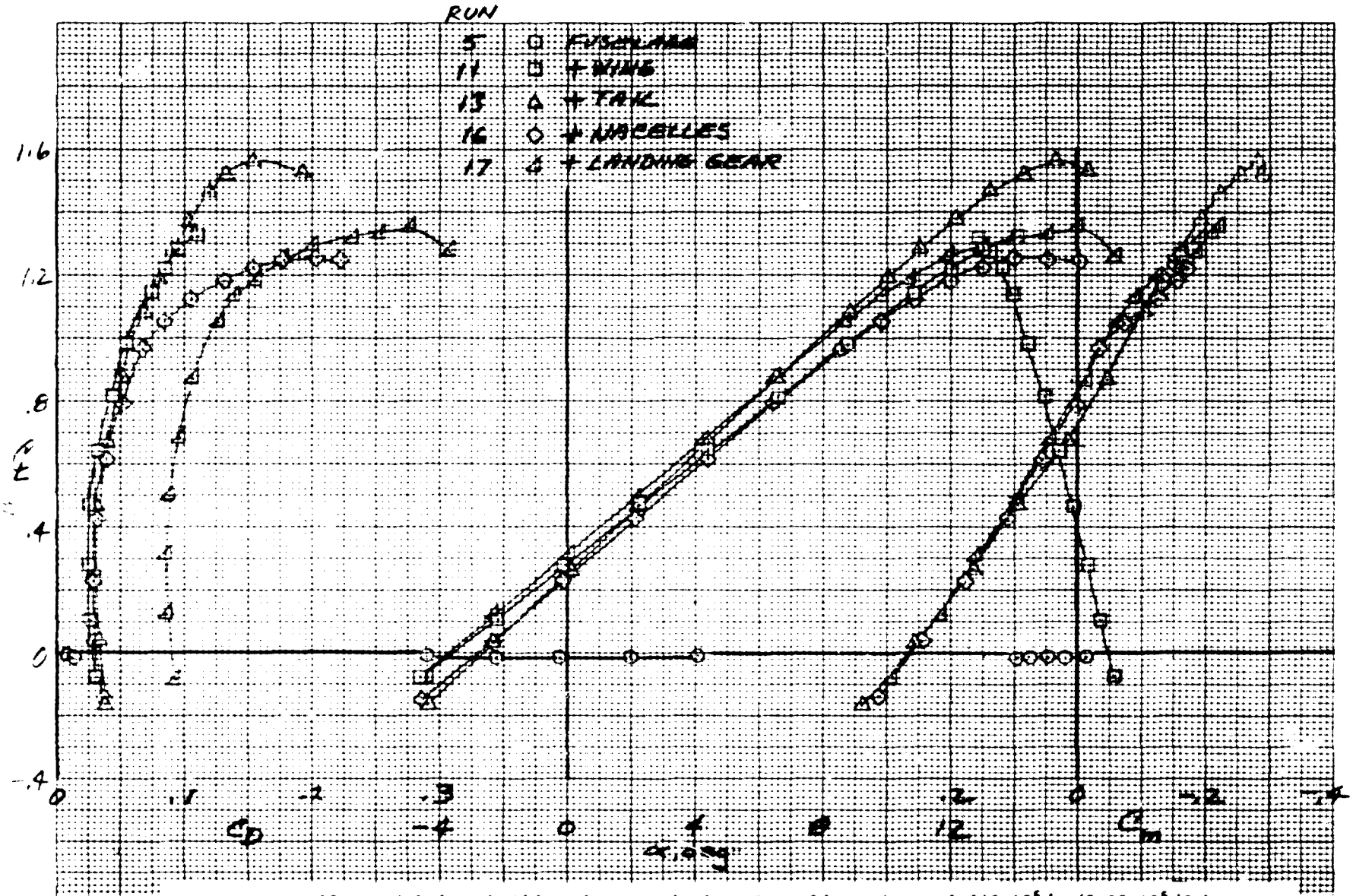

Figure 10.- Model drag-buildup characteristics; Reynolds number = 1.640×10^6/m (5.38×10^6/ft); q = 11,879.1 N/m^2 (248.1 psf).

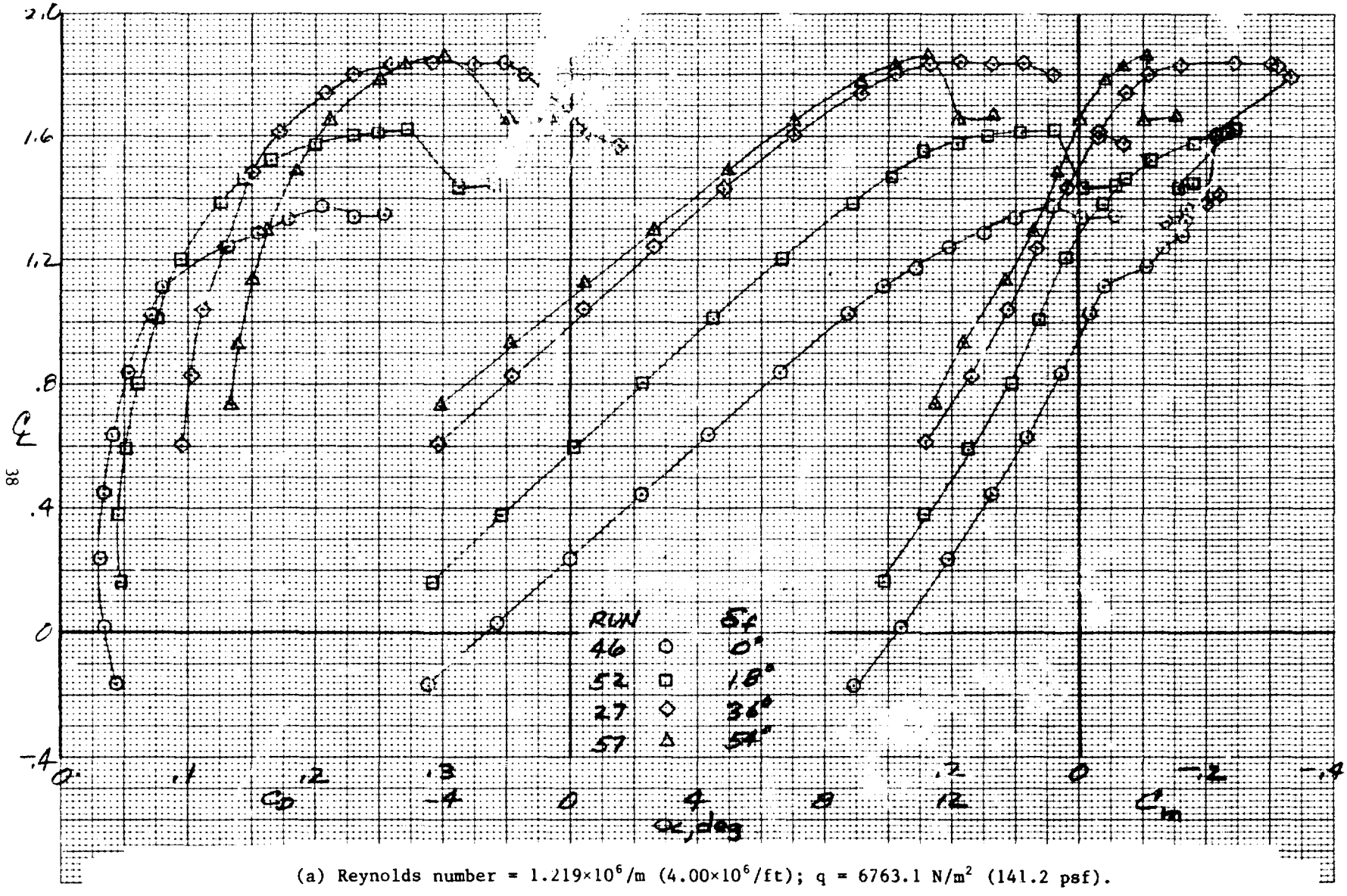

(a) Reynolds number = 1.219×10^6/m (4.00×10^6/ft); q = 6763.1 N/m^2 (141.2 psf).

Figure 11.- Effects of flap deflection on the longitudinal aerodynamic characteristics of the model; basic configuration.

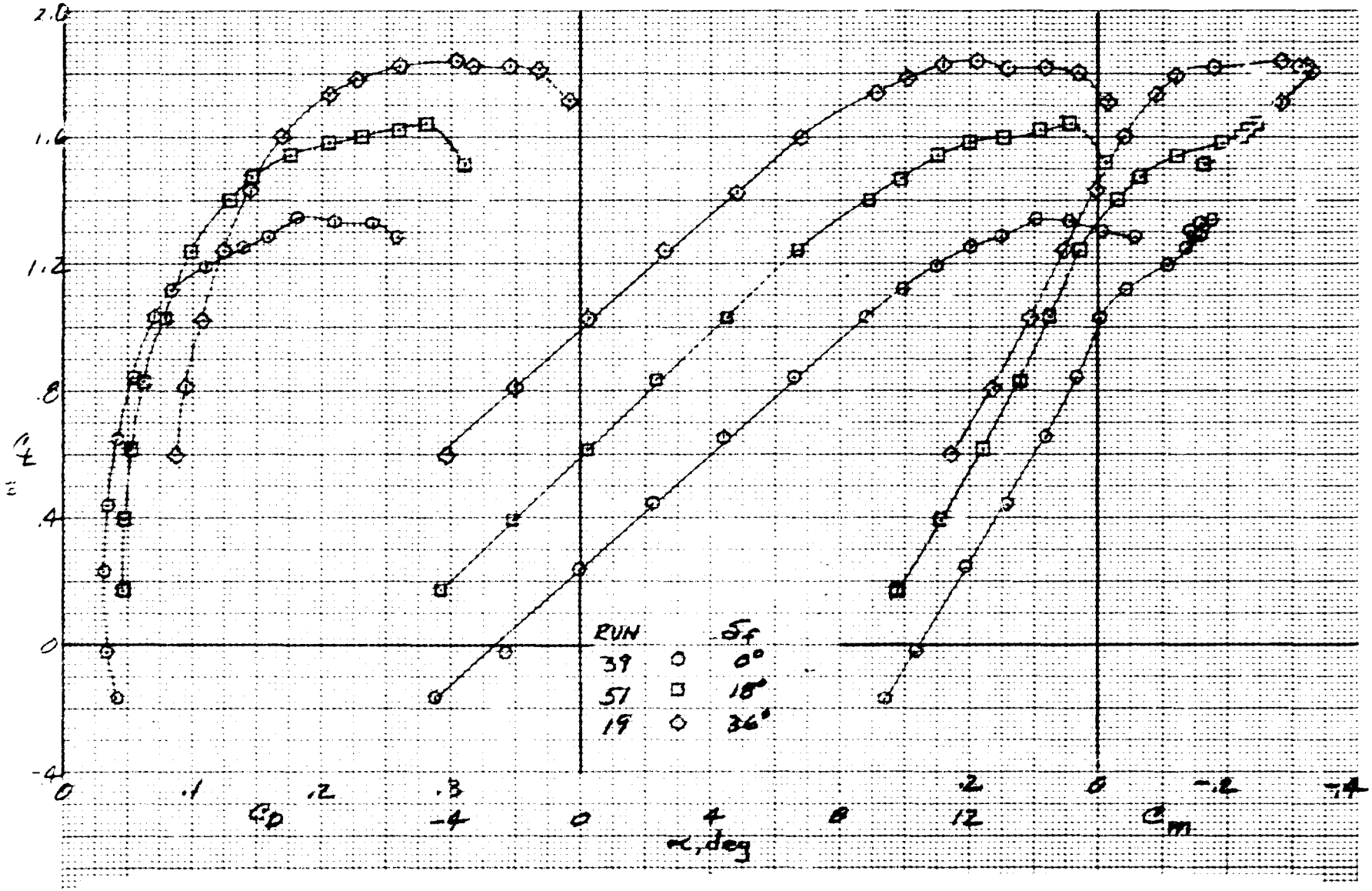

(b) Reynolds number = 1.646×10^6/m (5.40×10^6/ft); q = 12153.6 N/m^2 (253.8 psf).

Figure 11.- Concluded.

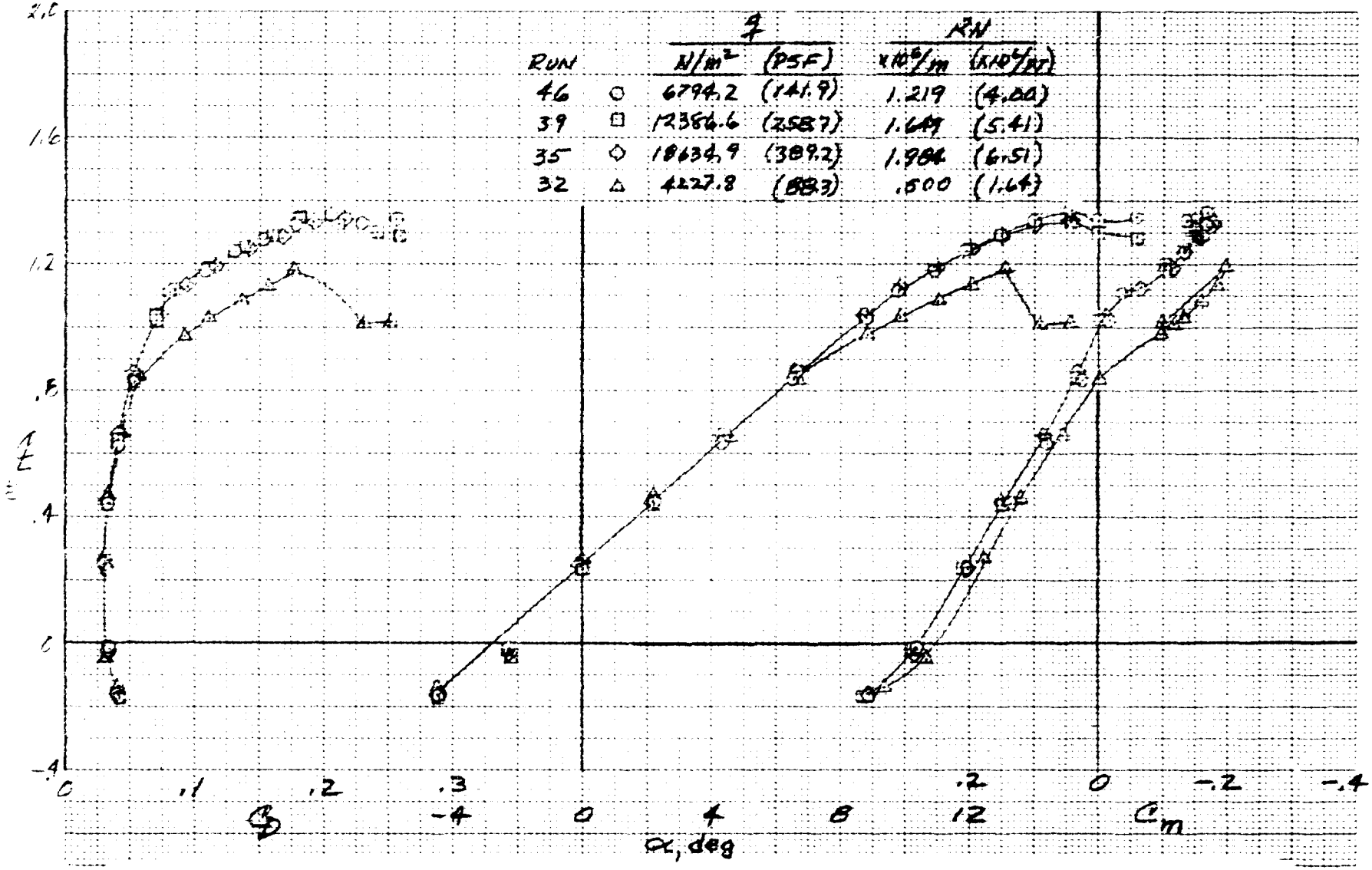

(a) $i_f = 0°$.

Figure 12.- Effects of Reynolds number on longitudinal aerodynamic characteristics; basic configuration.

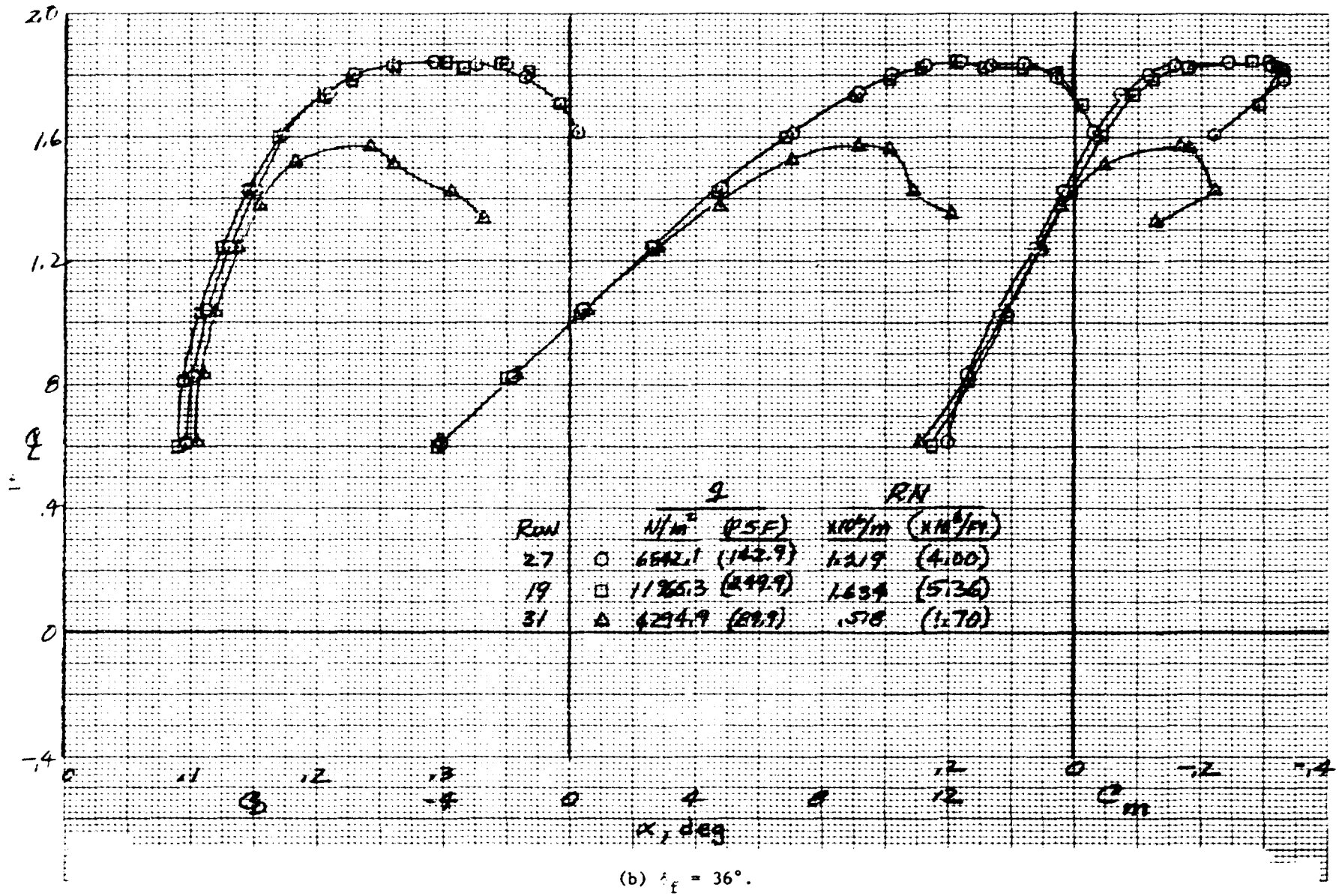

(b) δ_f = 36°.

Figure 12.- Concluded.

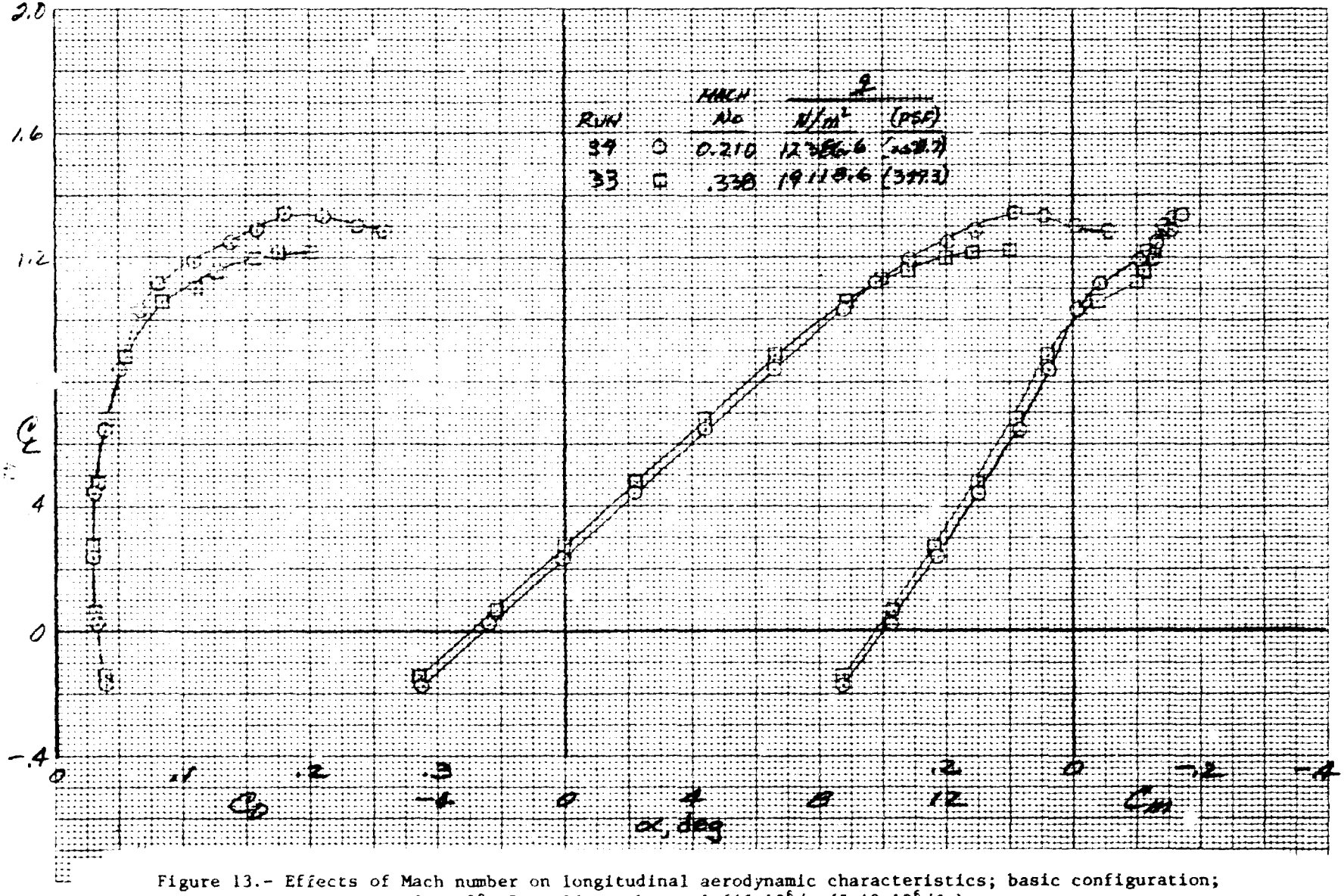

Figure 13.- Effects of Mach number on longitudinal aerodynamic characteristics; basic configuration; $\delta_f = 0°$; Reynolds number = 1.646×10^6/m (5.40×10^6/ft).

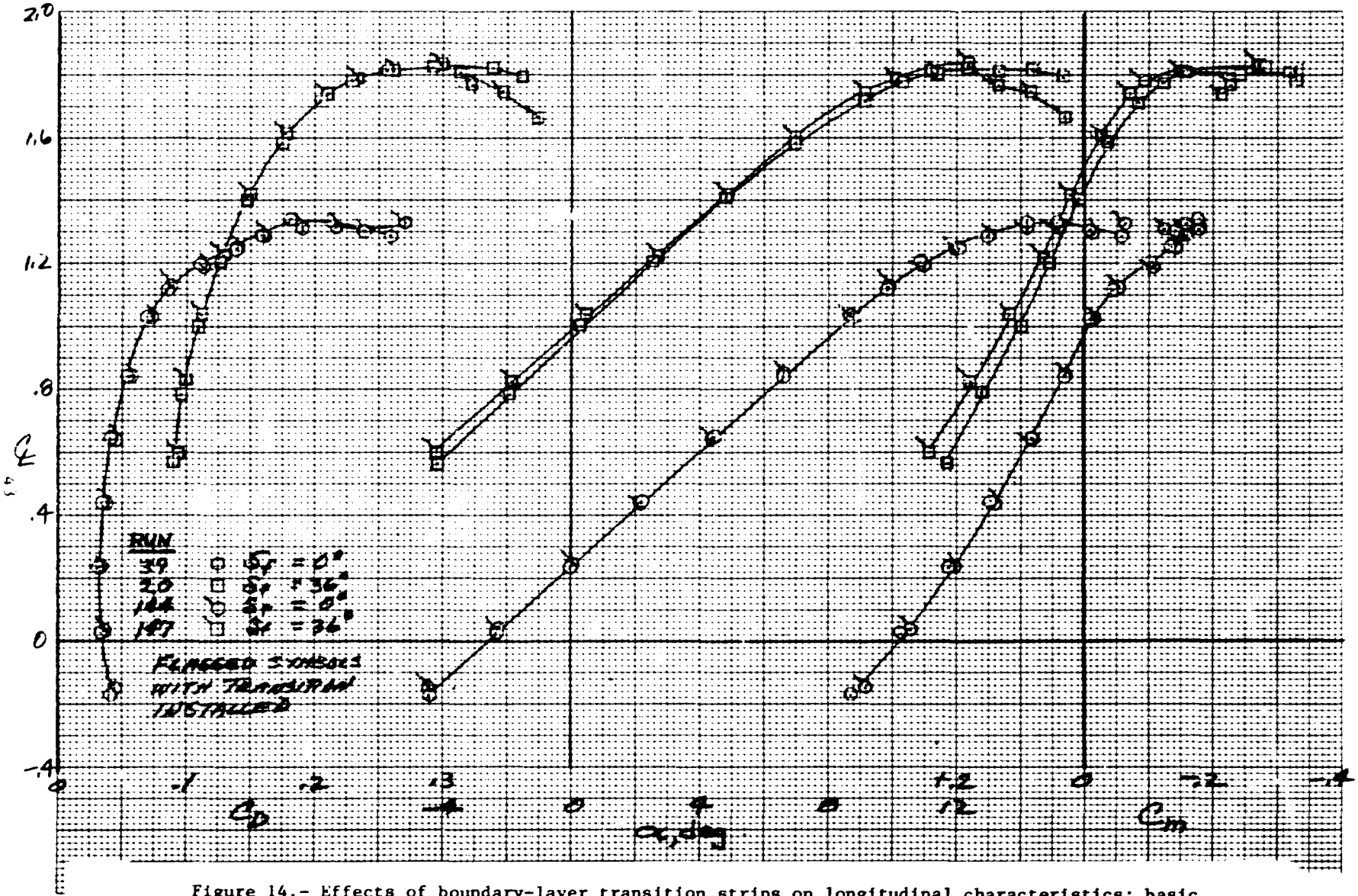

Figure 14.- Effects of boundary-layer transition strips on longitudinal characteristics; basic configuration; Reynolds number = 1.640×10^6/m (5.38×10^6/ft); q = 12226.2 N/m^2 (255.4 psf).

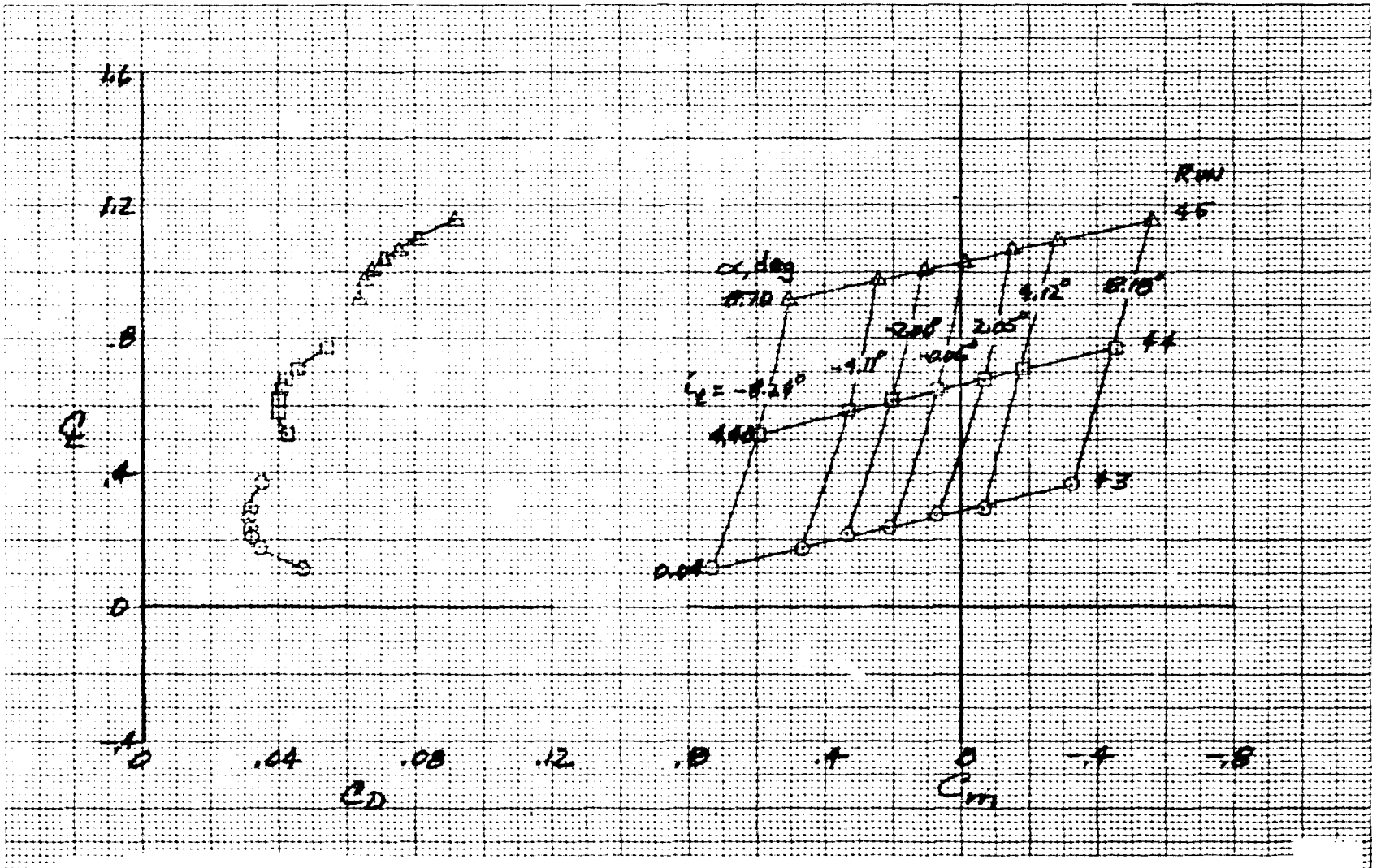

(a) $i_f = 0°$; q = 12,233.4 N/m^2 (255.5 psf); Reynolds number = 1.649×10^6/m (5.41×10^6/ft).

Figure 15.- Effects of tail incidence on longitudinal aerodynamic characteristics; basic configuration.

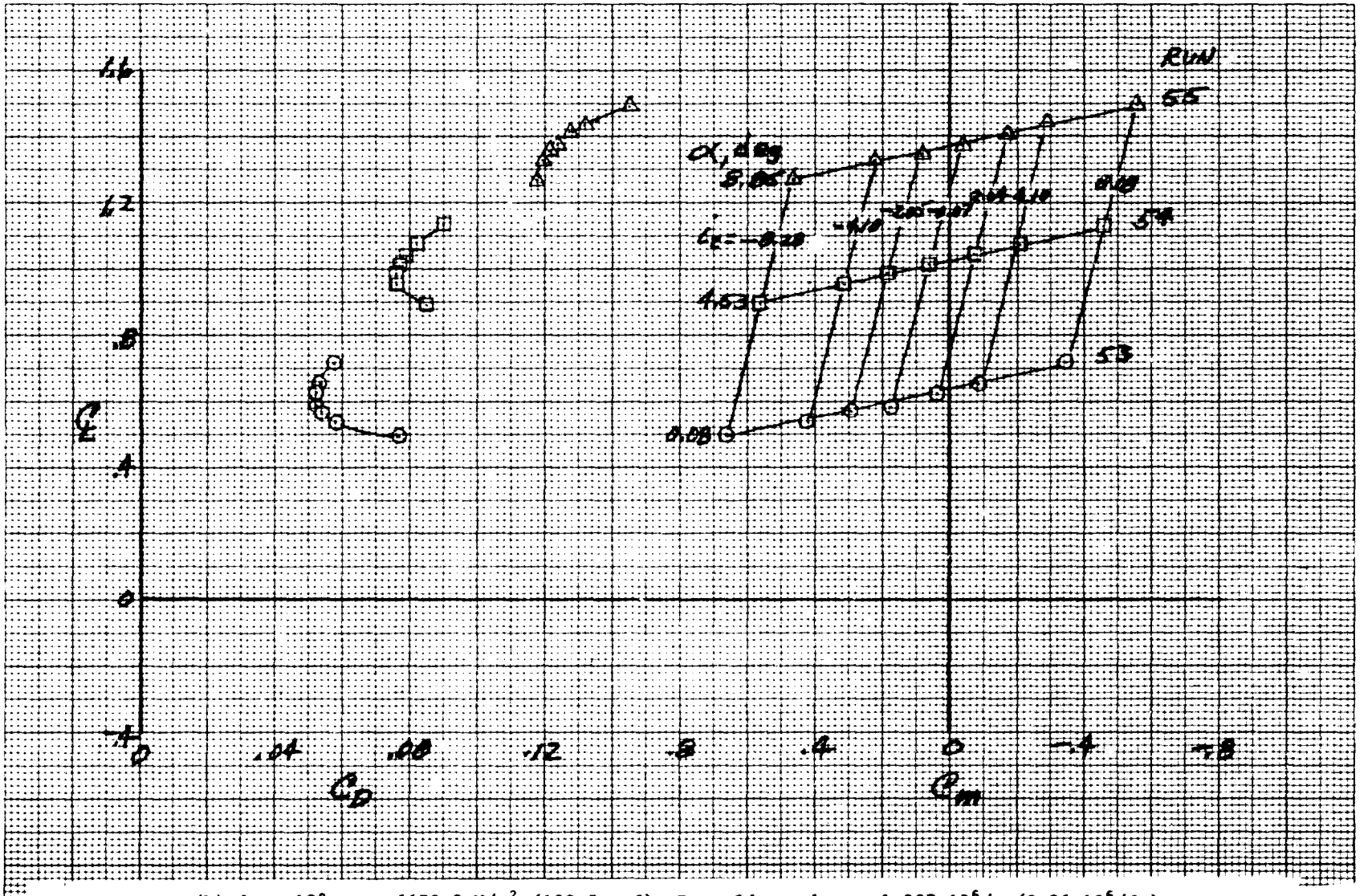

(b) δ_f = 18°; q = 6679.3 N/m^2 (139.5 psf); Reynolds number = 1.207×10^6/m (3.96×10^6/ft).

Figure 15.- Continued.

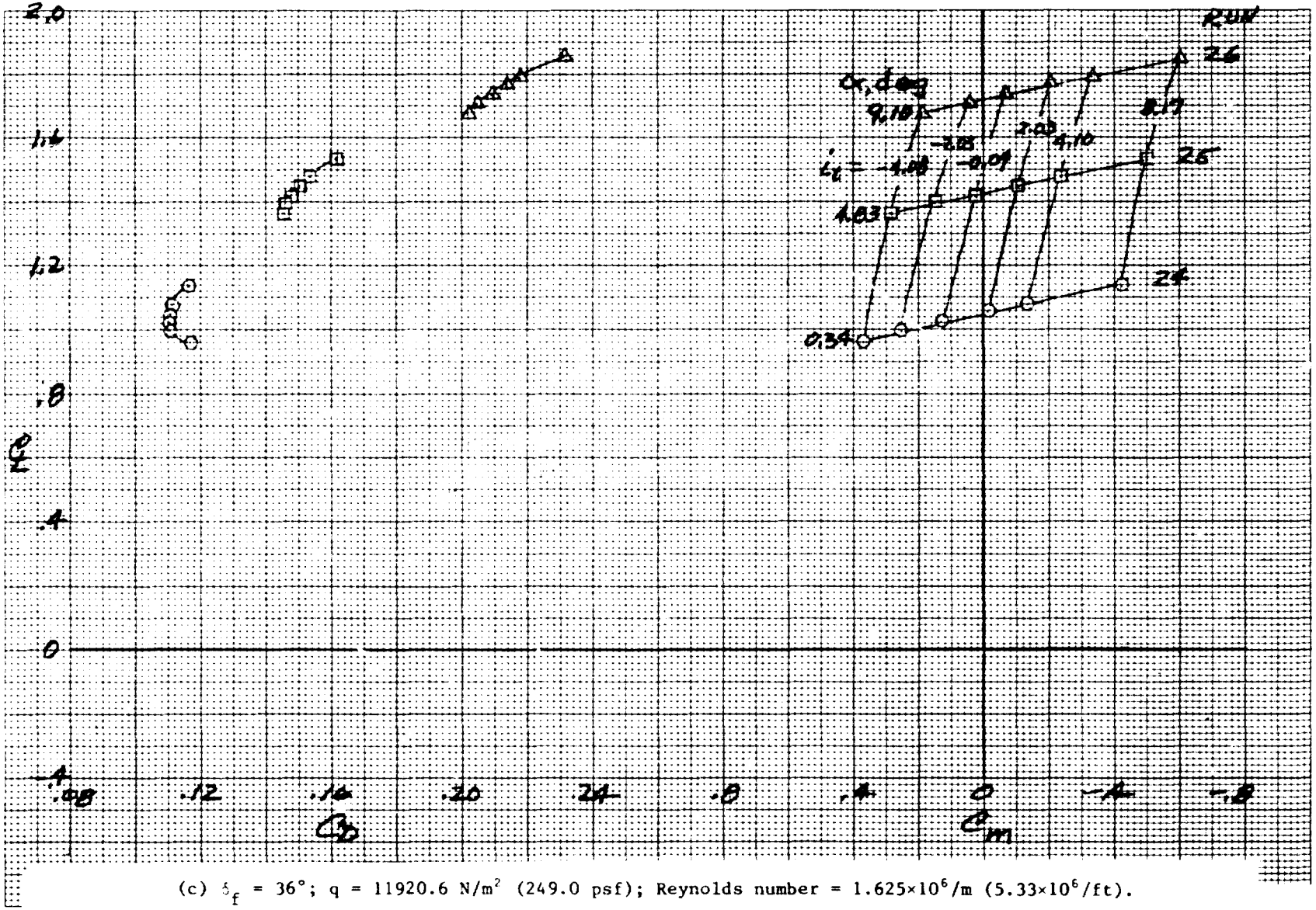

(c) δ_f = 36°; q = 11920.6 N/m^2 (249.0 psf); Reynolds number = 1.625×10^6/m (5.33×10^6/ft).

Figure 15.- Concluded.

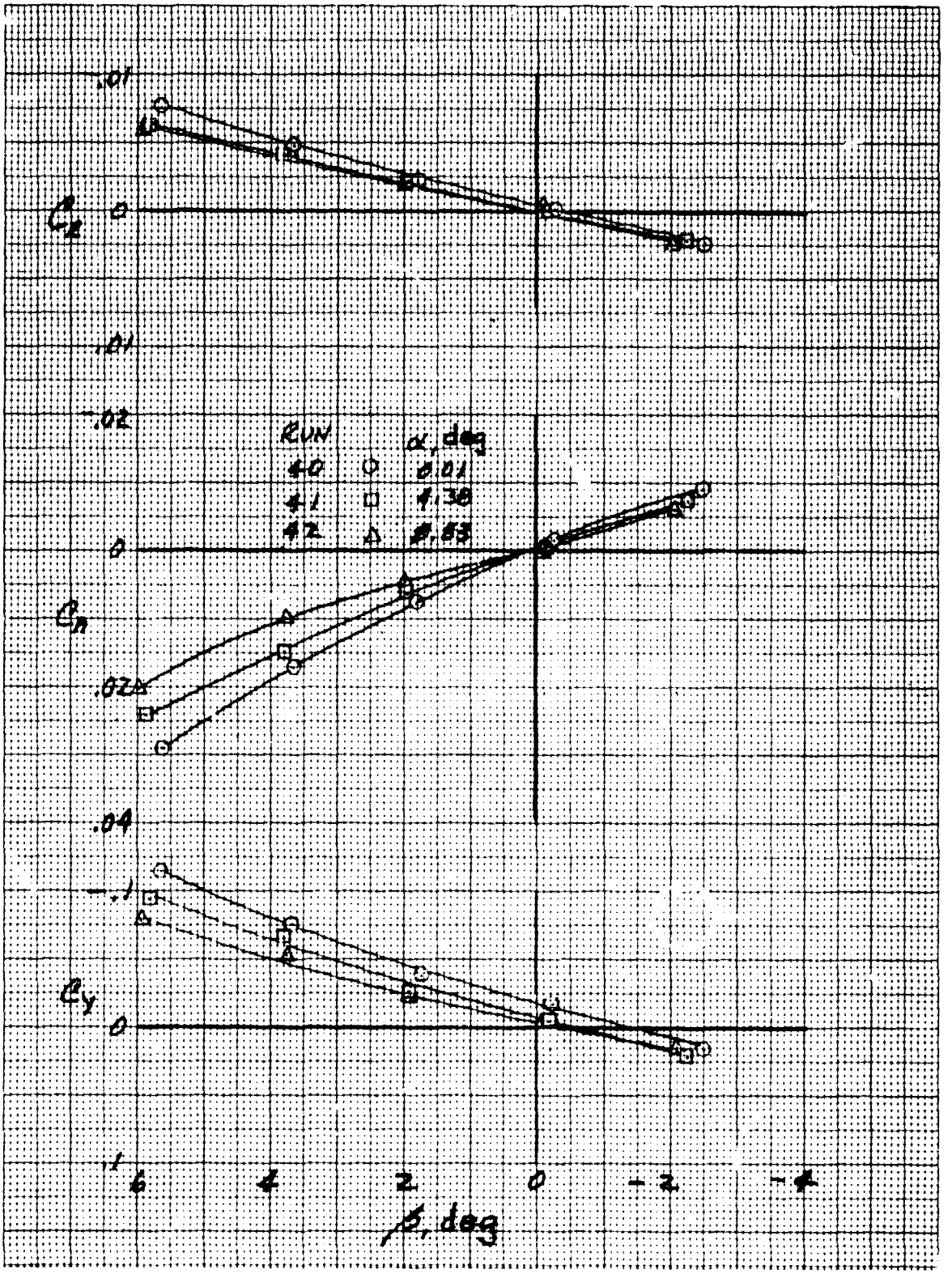

(a) $\delta_f = 0°$; q = 12,233 N/m^2 (255.5 psf); Reynolds number = 1.219×10^6/m (5.40×10^6/ft).

Figure 16.- Variation of side-force, yawing-moment, and rolling-moment coefficients with sideslip; basic configuration.

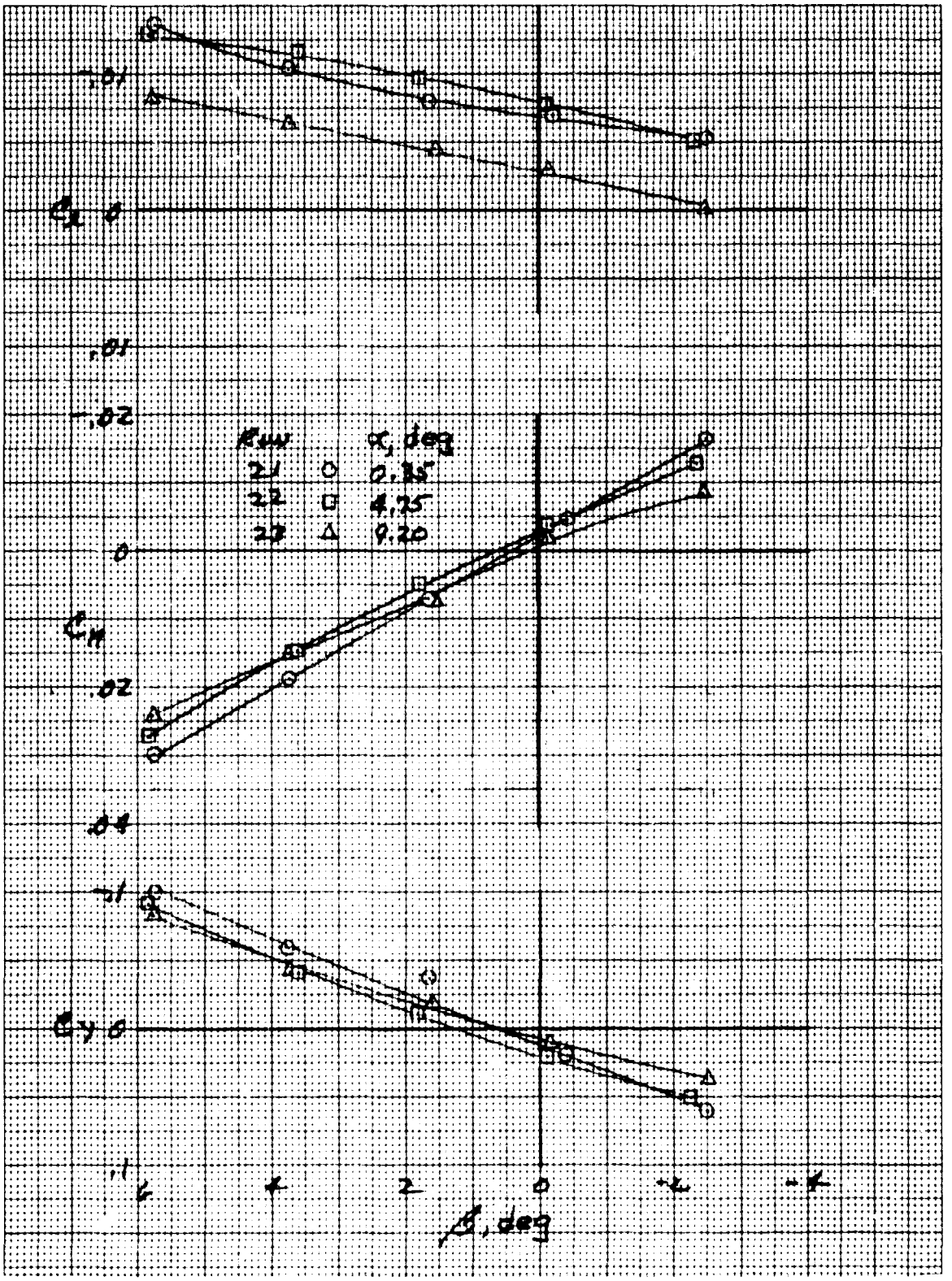

(b) δ_f = 36°; q = 11858.3 N/m² (247.6 psf); Reynolds number = 1.625×10^6/m (5.33×10^6/ft)

Figure 16.- Concluded.

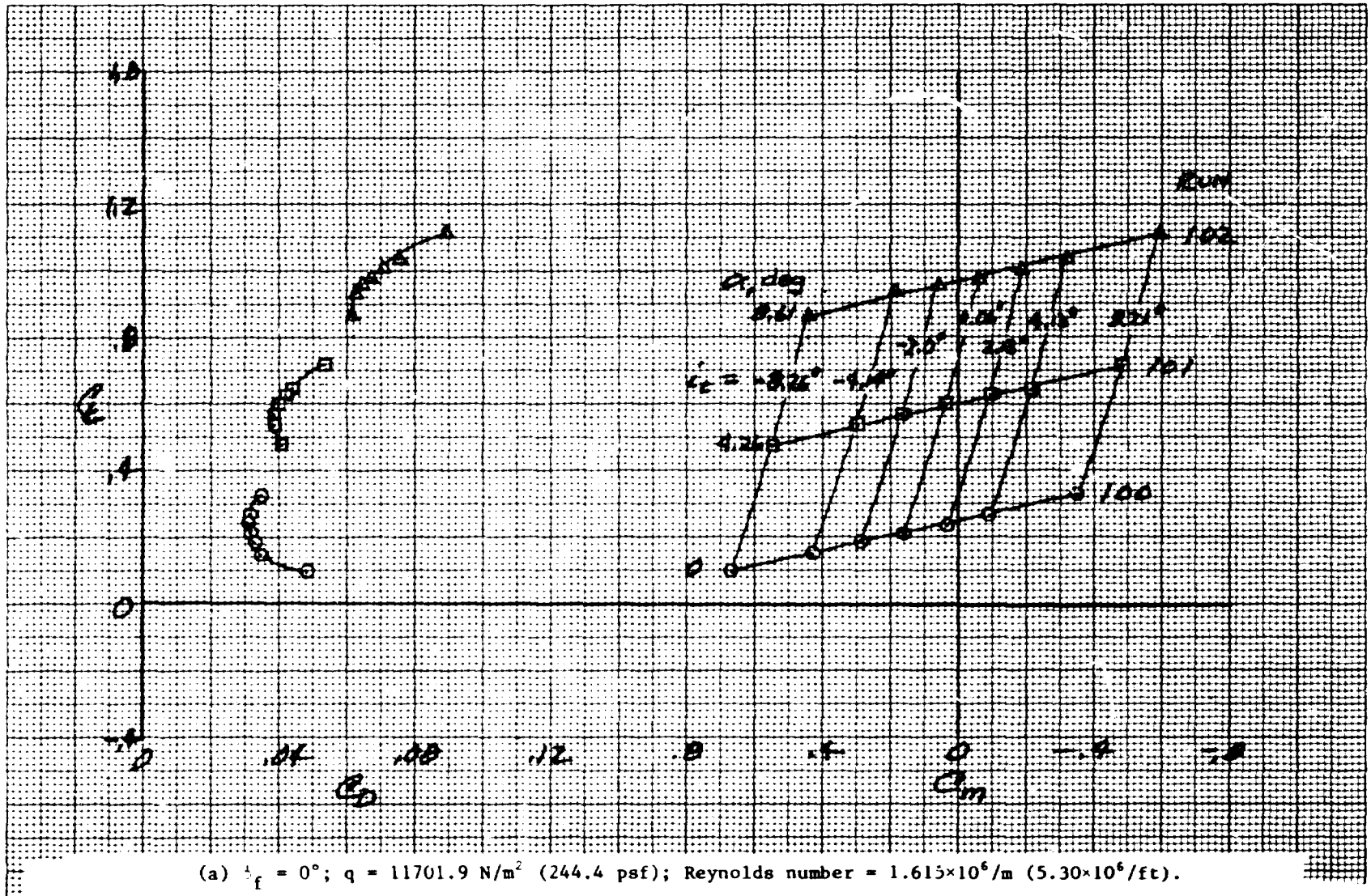

(a) $i_f = 0°$; $q = 11701.9\ N/m^2$ (244.4 psf); Reynolds number = $1.615 \times 10^6/m$ ($5.30 \times 10^6/ft$).

Figure 17.- Effects of tail incidence on the longitudinal aerodynamic characteristics, low-nacelle configuration.

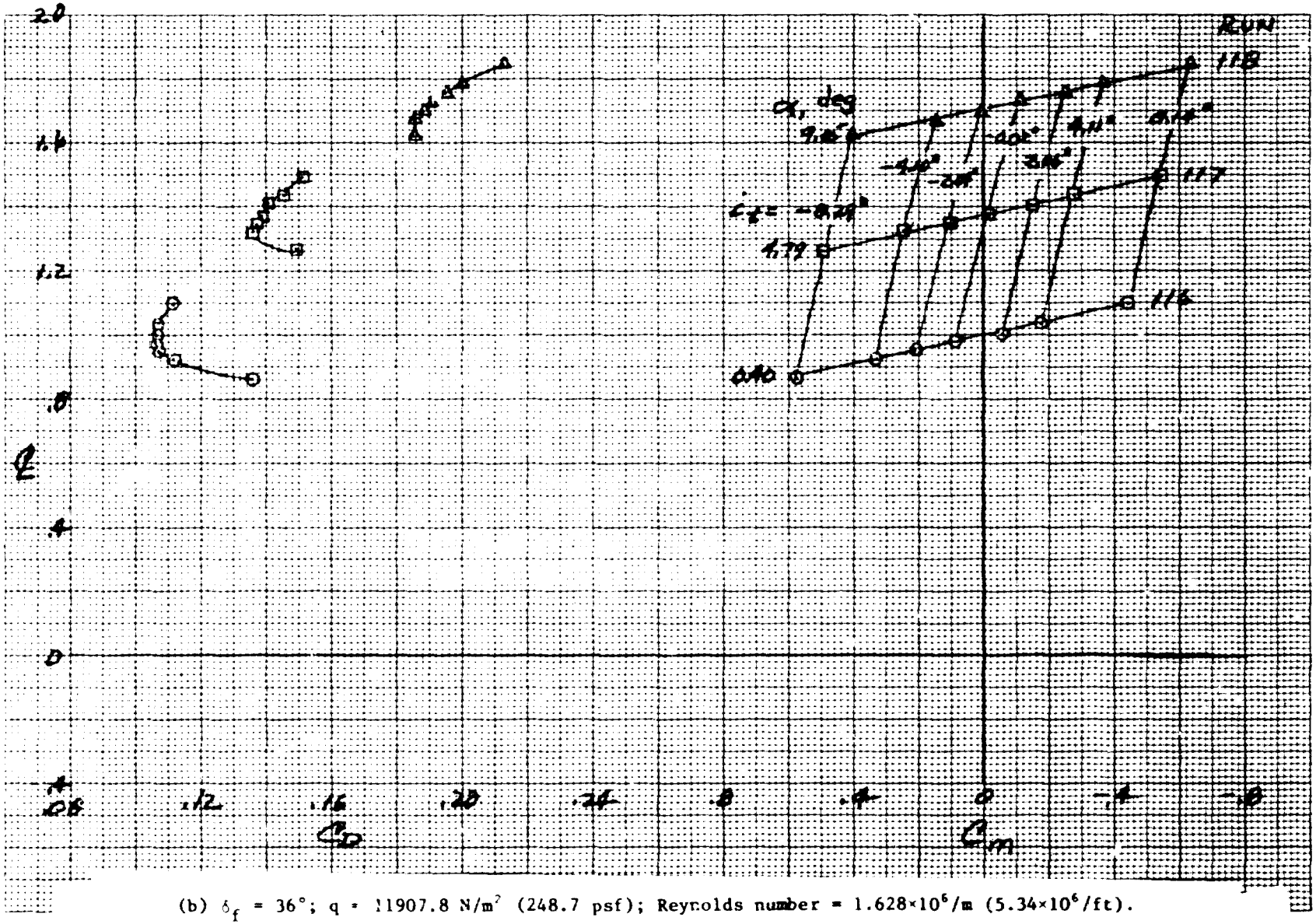

(b) δ_f = 36°; q = 11907.8 N/m^2 (248.7 psf); Reynolds number = 1.628×10^6/m (5.34×10^6/ft).

Figure 17.- Concluded.

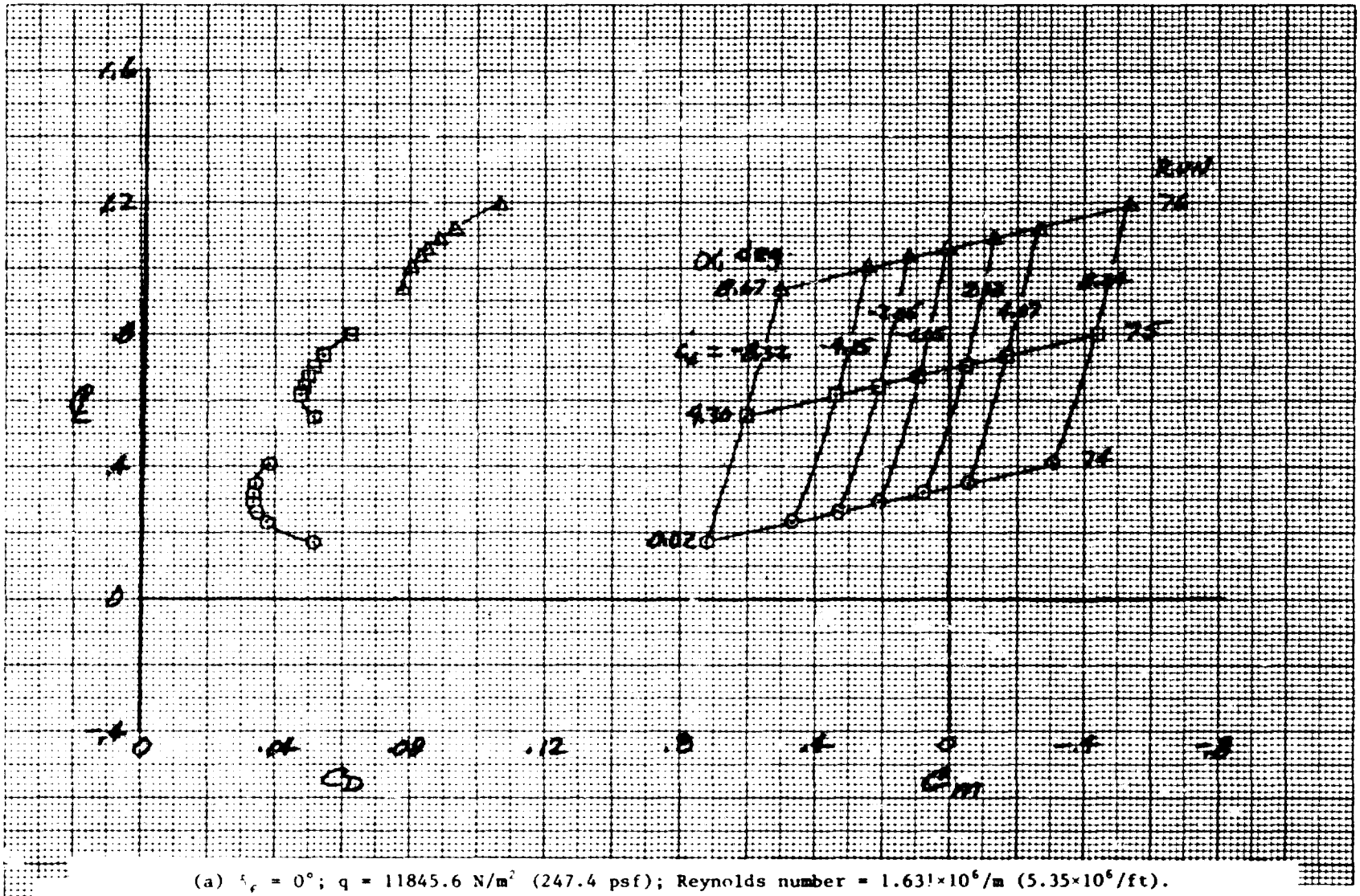

(a) i_t = 0°; q = 11845.6 N/m^2 (247.4 psf); Reynolds number = 1.631×10^6/m (5.35×10^6/ft).

Figure 18.- Effects of tail incidence on longitudinal aerodynamic characteristics; high-nacelle configuration.

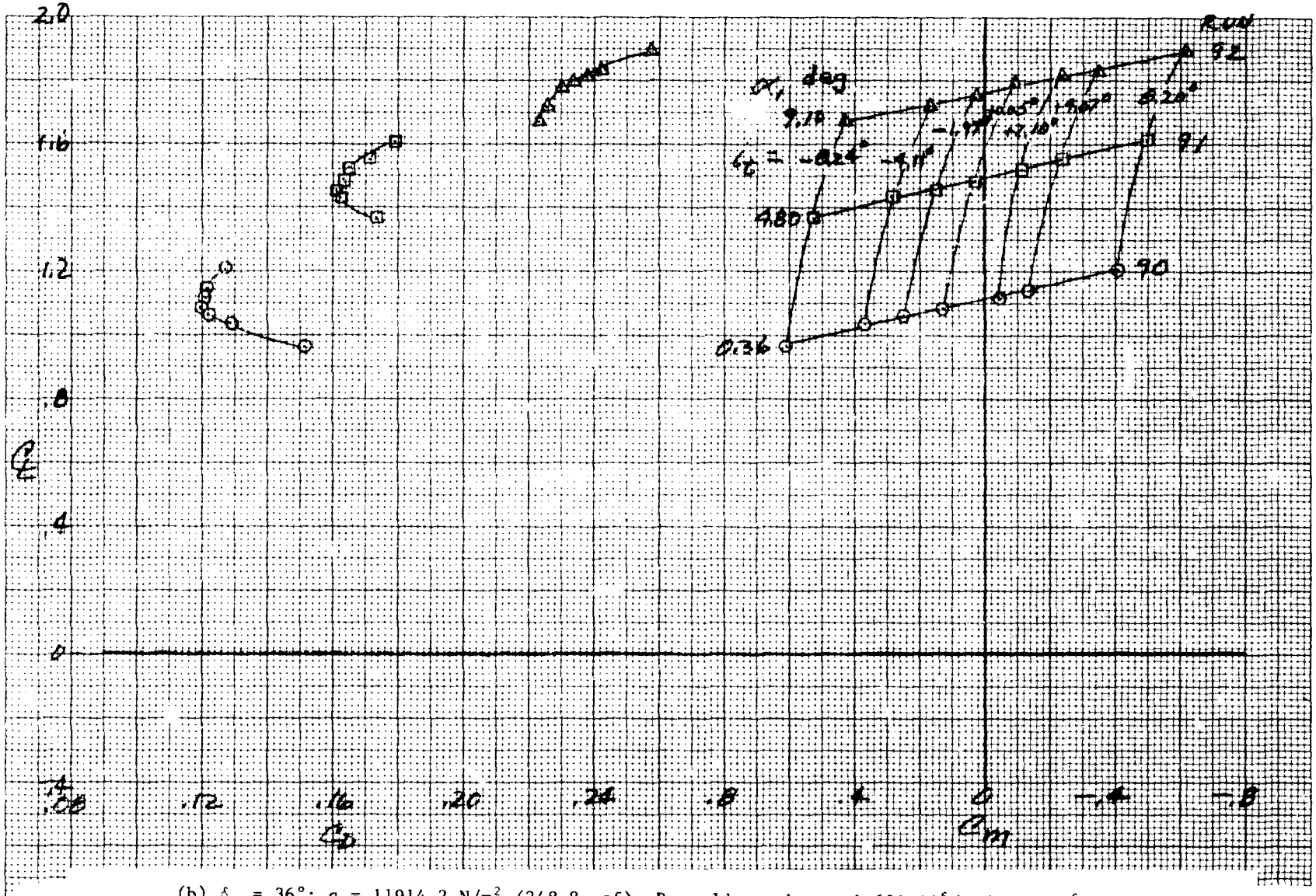

(b) δ_f = 36°; q = 11914.2 N/m^2 (248.8 psf); Reynolds number = 1.631×10^6/m (5.35×10^6/ft).

Figure 18.- Concluded.

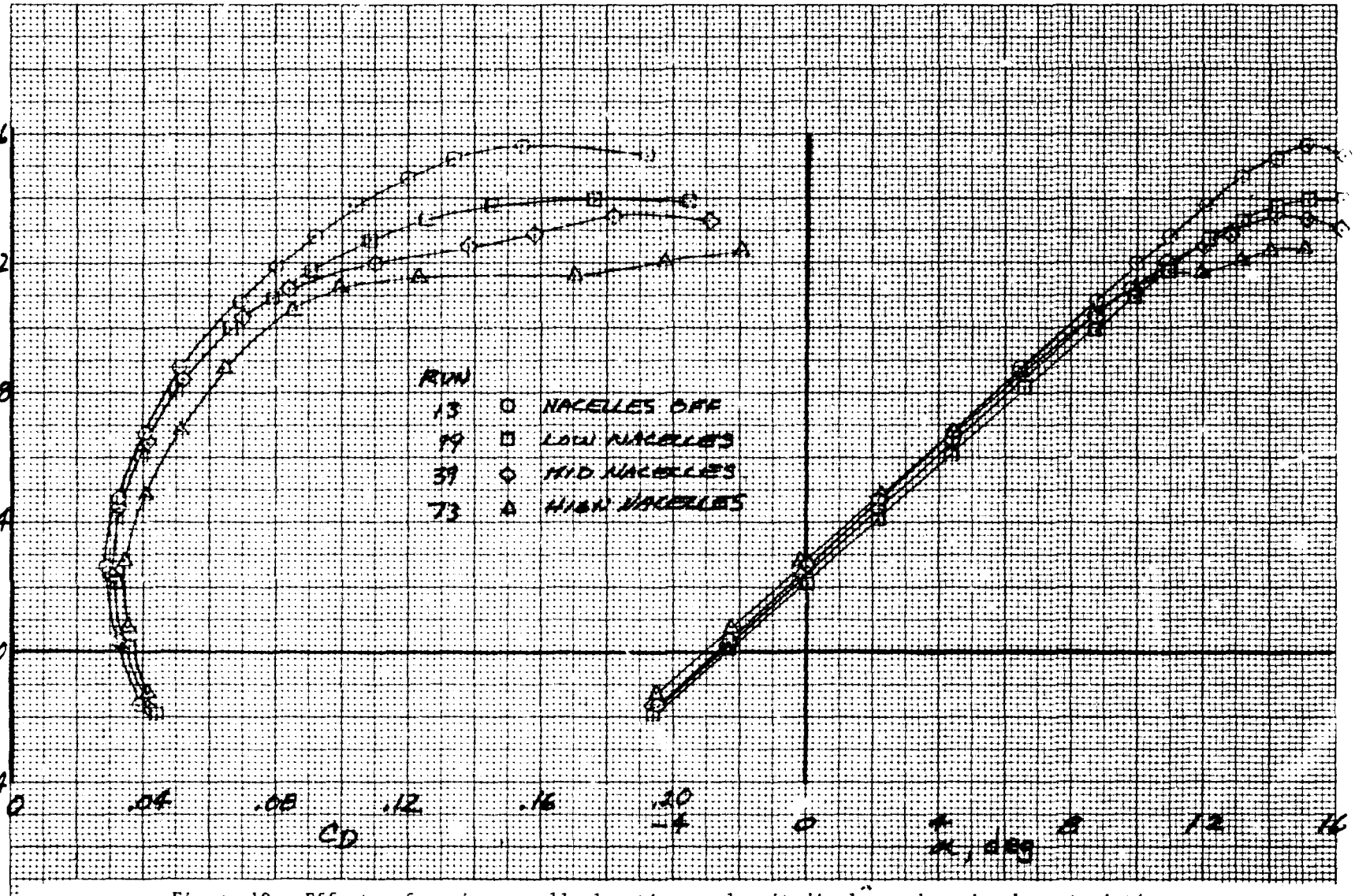

Figure 19.- Effects of engine-nacelle location on longitudinal aerodynamic characteristics; $q = 11{,}941.3\ N/m^2$ (249.4 psf); Reynolds number = 1.637×10^6/m (5.37×10^6/ft).

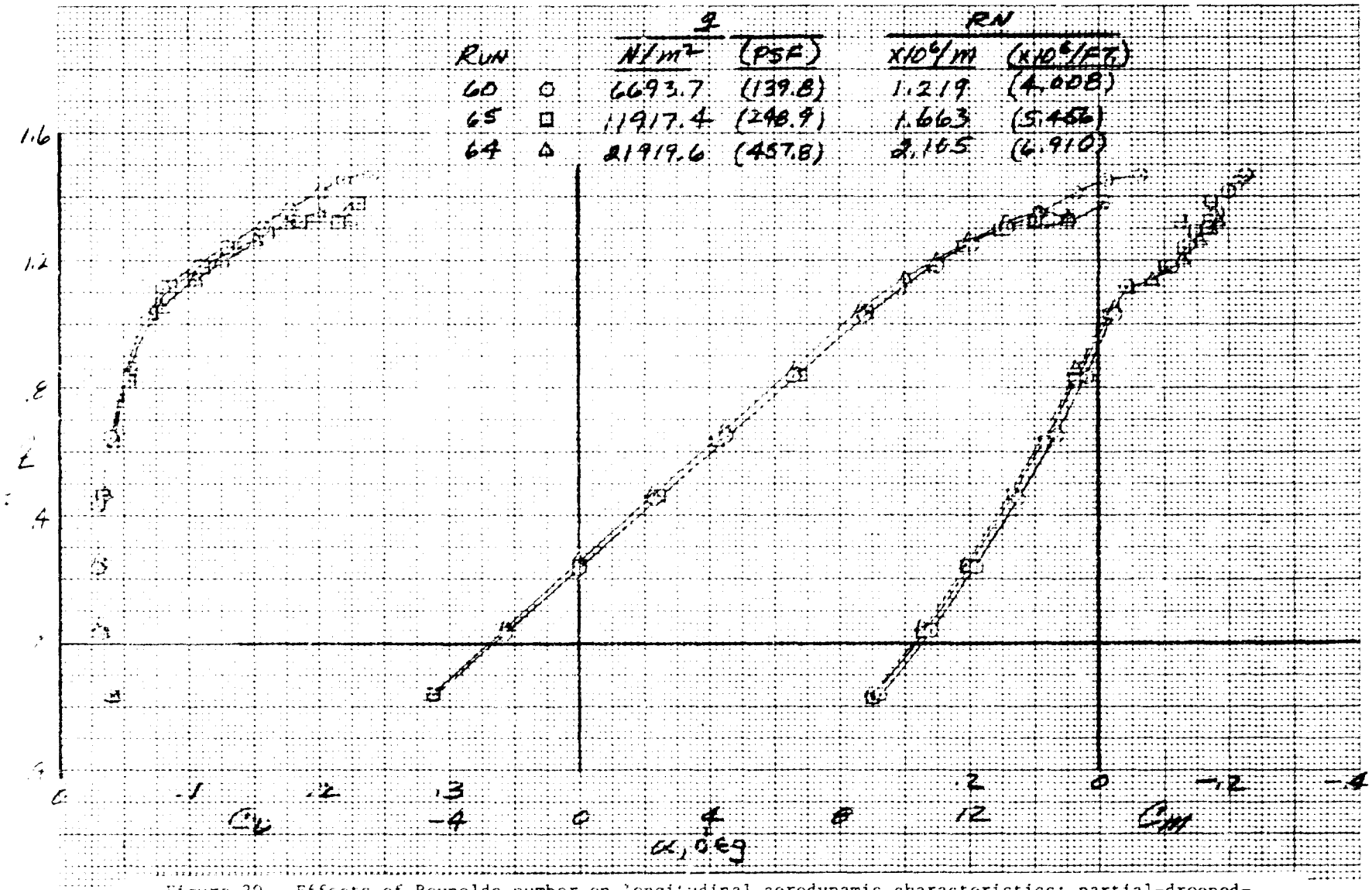

Figure 20.- Effects of Reynolds number on longitudinal aerodynamic characteristics; partial-drooped-leading-edge configuration; $\delta_f = 0°$.

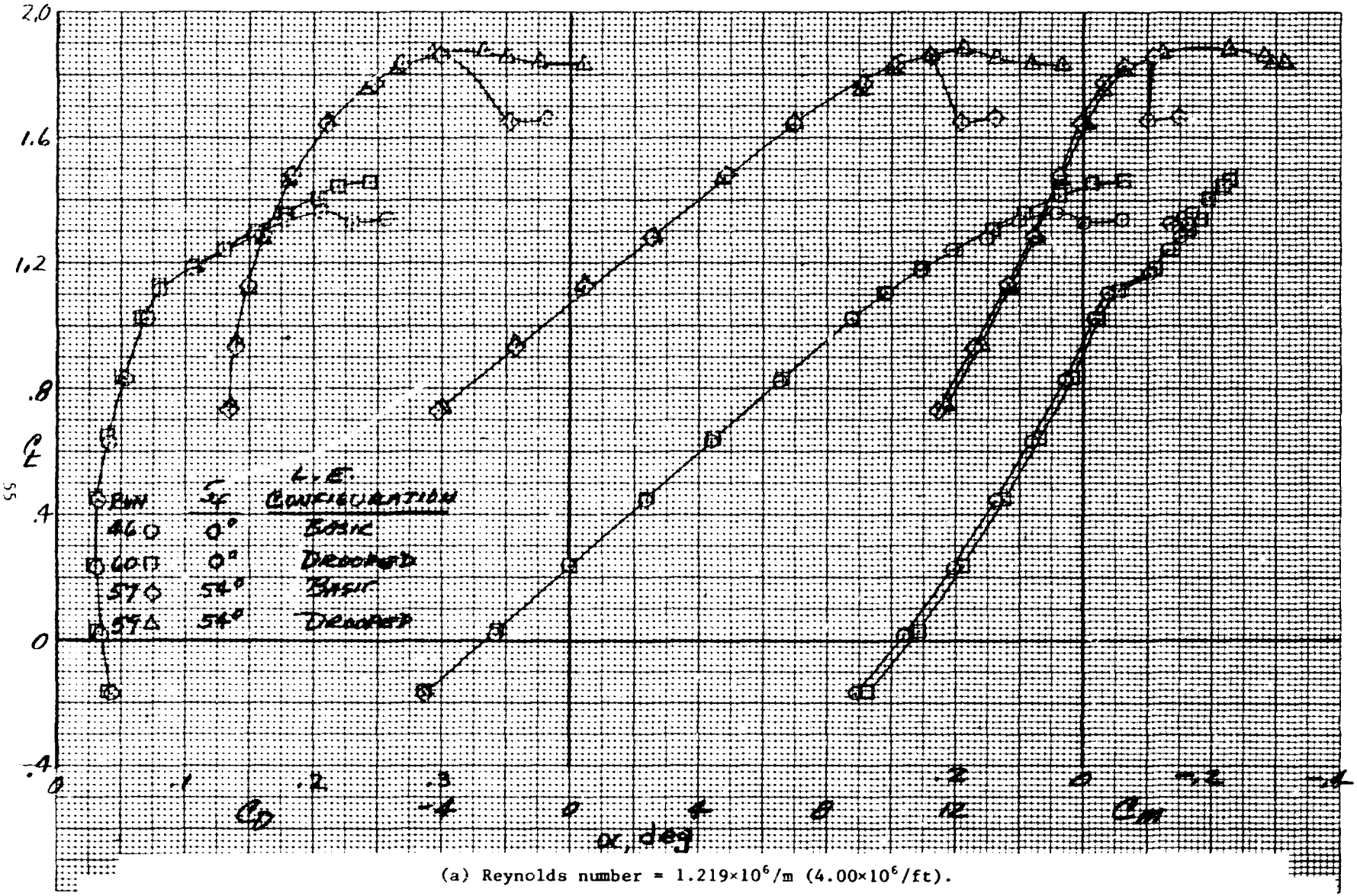

(a) Reynolds number = 1.219×10^6/m (4.00×10^6/ft).

Figure 21.- Comparison of longitudinal characteristics of basic and partial-span drooped-leading-edge configurations; q = 6,746.3 N/m^2 (140.9 psf).

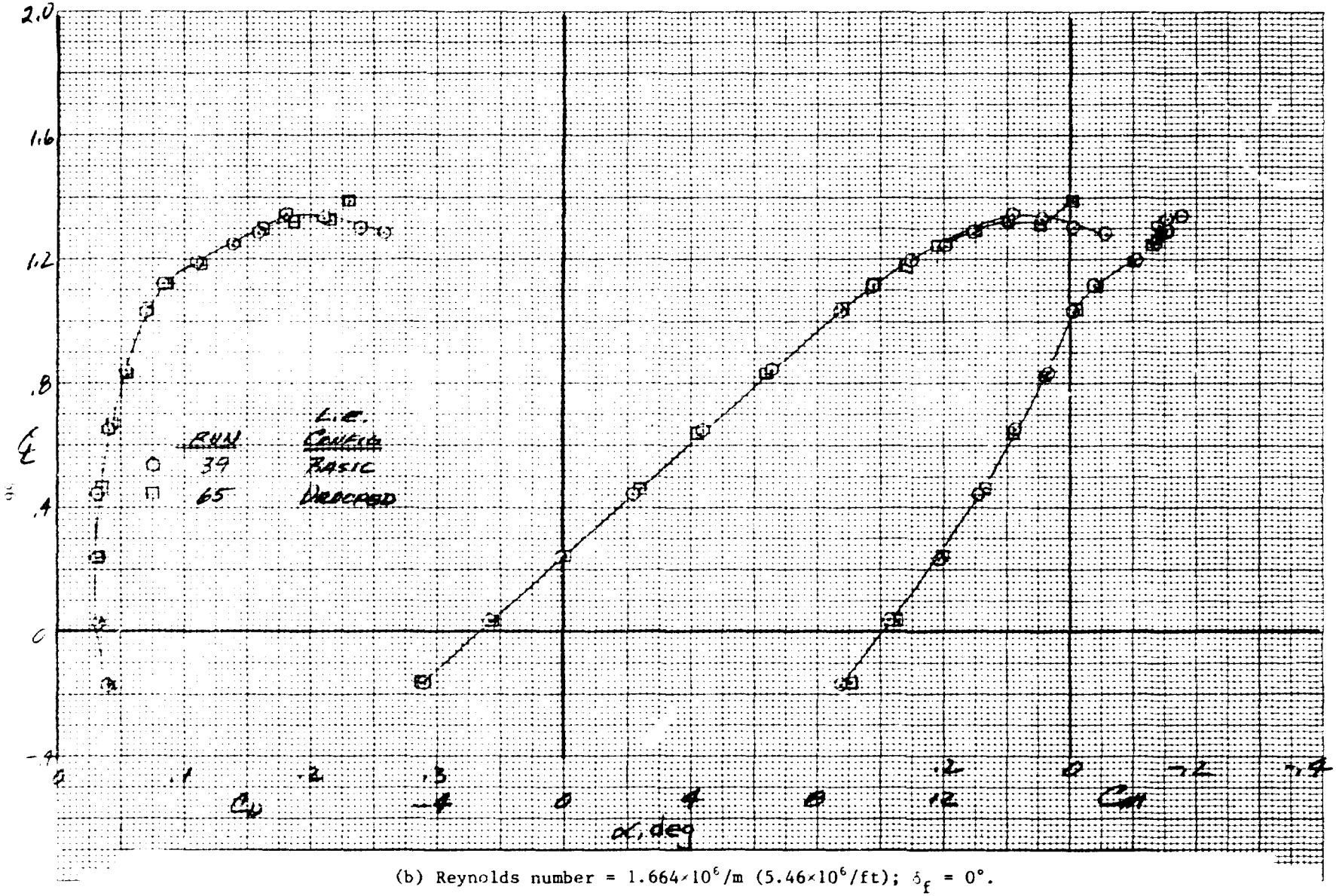

(b) Reynolds number = 1.664×10^6/m (5.46×10^6/ft); $\delta_f = 0°$.

Figure 21.- Continued.

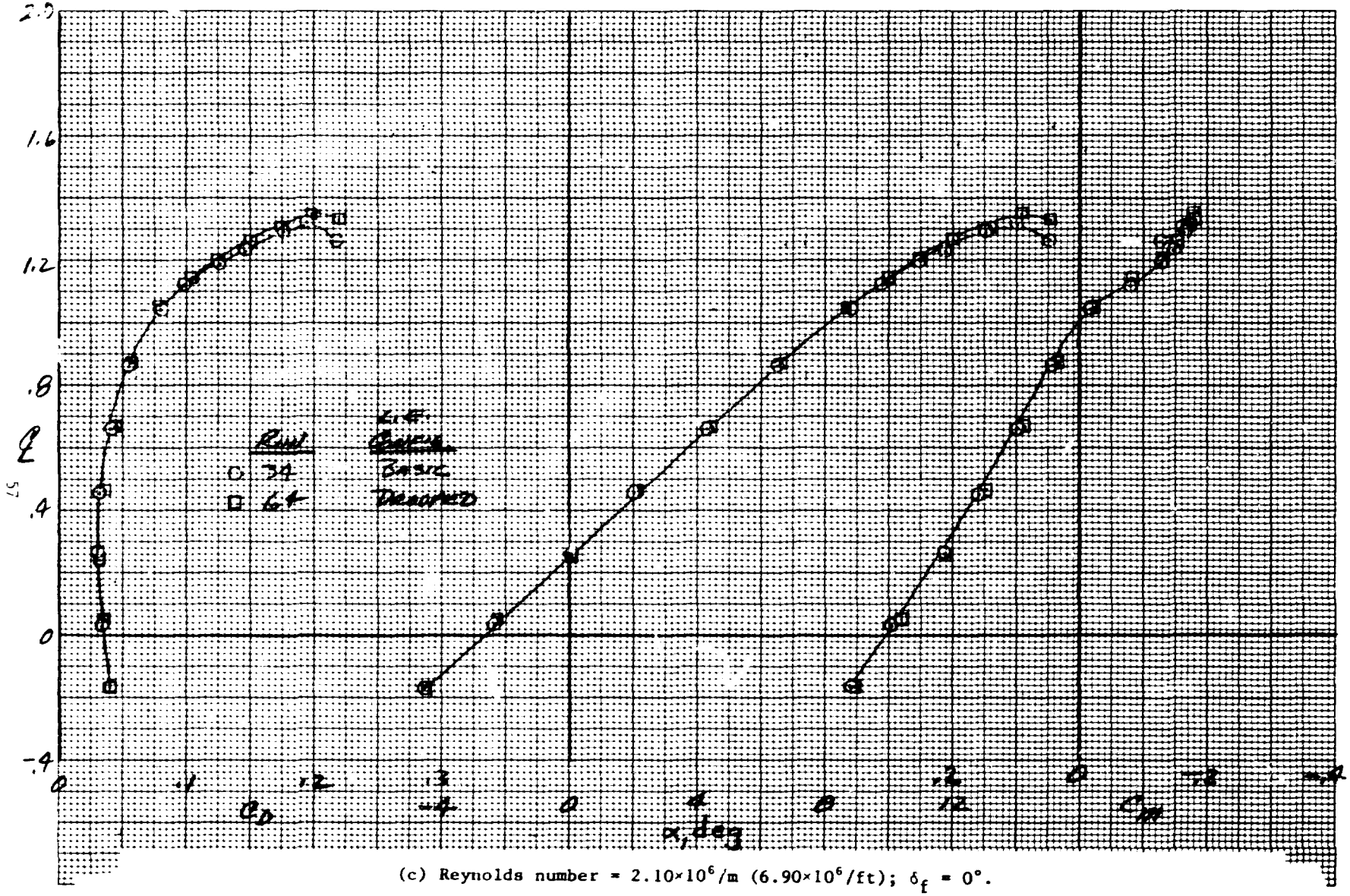

(c) Reynolds number = 2.10×10^6/m (6.90×10^6/ft); $\delta_f = 0°$.

Figure 21.- Concluded.

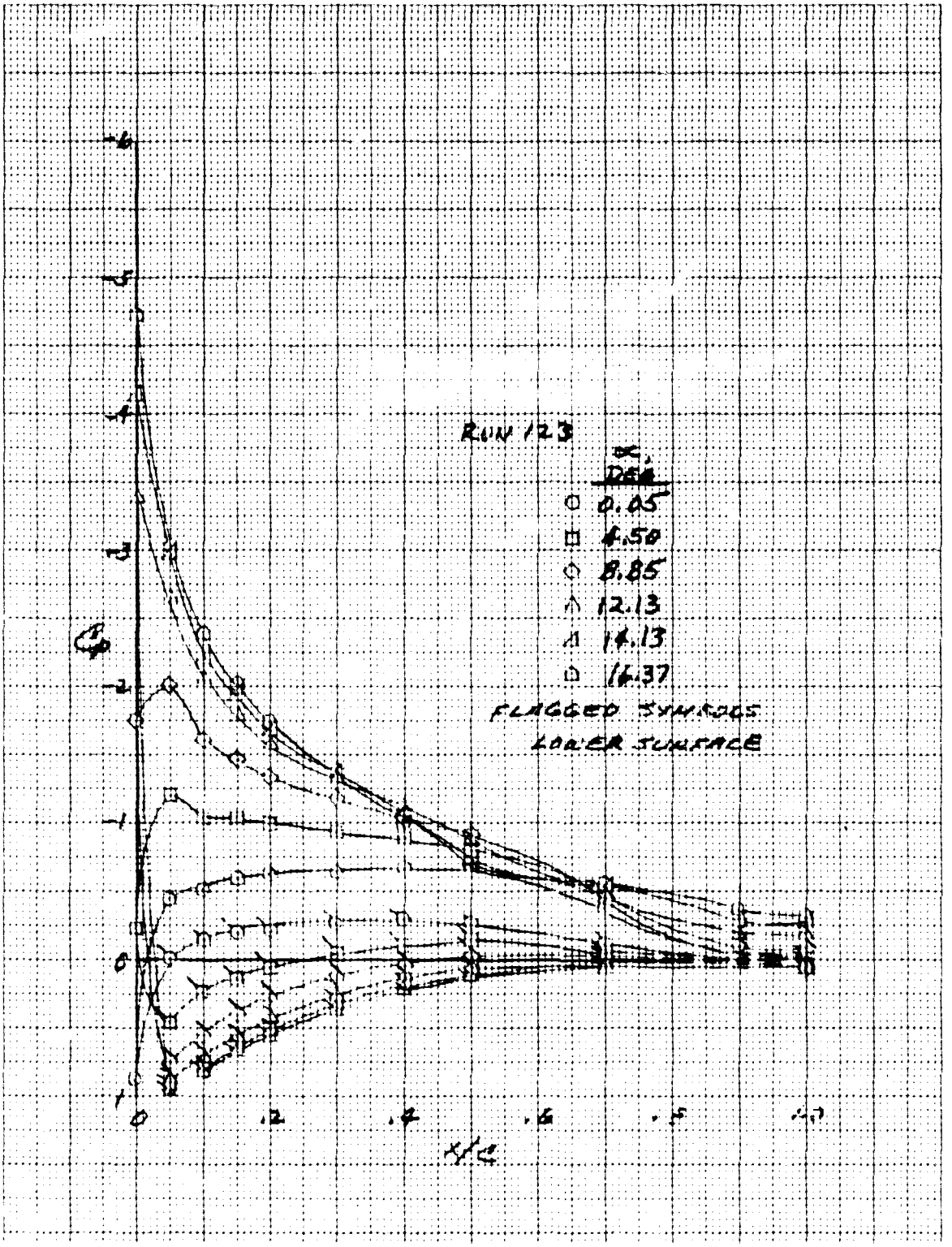

(a) Left-wing pressure strap 45 cm (18 in.) from fuselage centerline (outboard of nacelle).

Figure 22.- Model pressure distribution with wing-body configuration; $\delta_f = 0°$; $q = 11567.9$ N/m^2 (241.6 psf); Reynolds number = 1.628×10^6/m (5.34×10^6/ft).

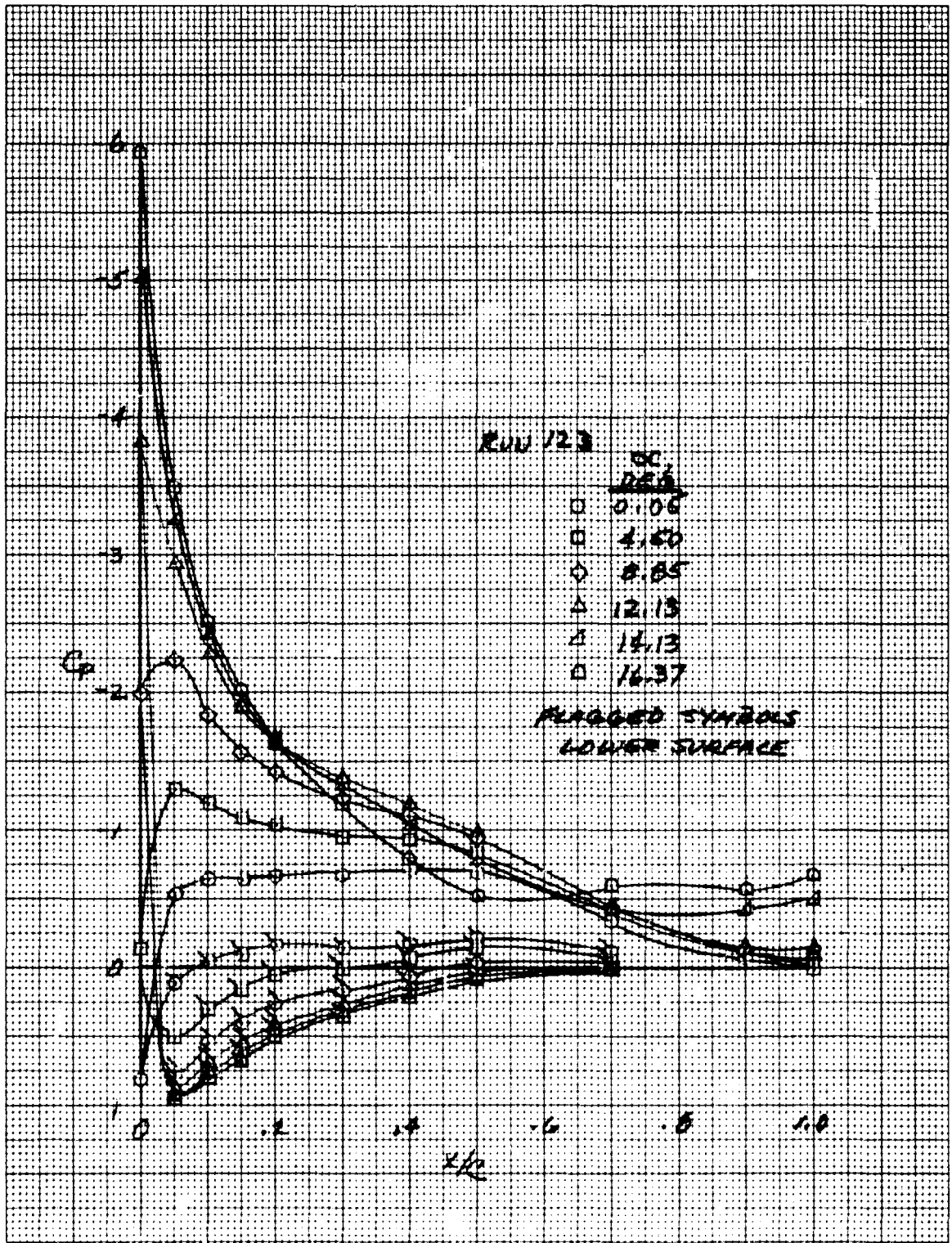

(b) Right-wing pressure strap 22.5 cm (9 in.) from fuselage centerline (inboard of nacelle).

Figure 22.- Concluded.

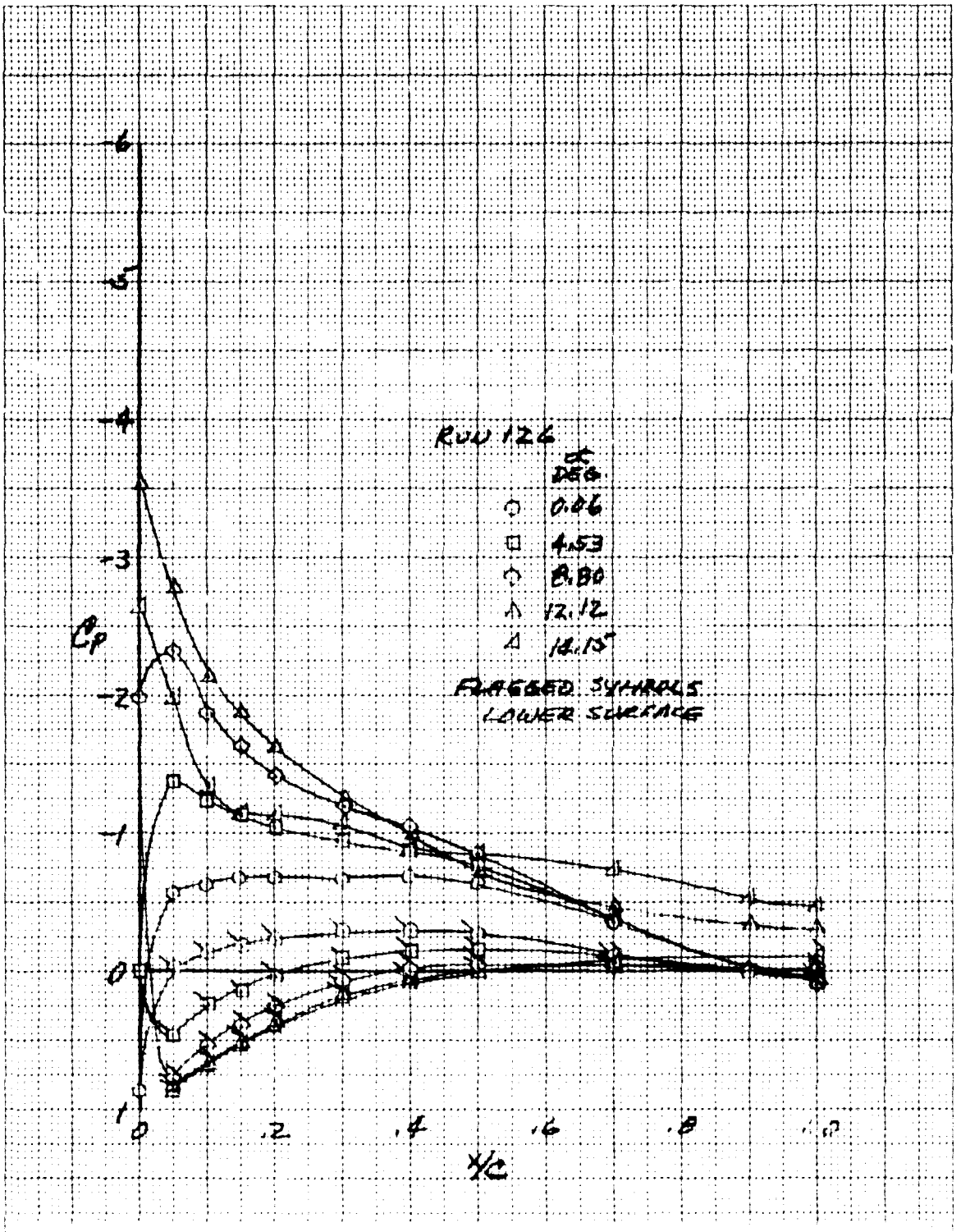

(a) Left-wing pressure strap 45 cm (18 in.) from fuselage centerline (outboard of nacelle).

Figure 23.- Model pressure distribution with wing-body-midnacelle configuration; $\alpha_t = 0°$; q = 11740.2 N/m² (245.2 psf); Reynolds number = $1.618 \cdot 10^7$/m ($5.31 \cdot 10^6$/ft).

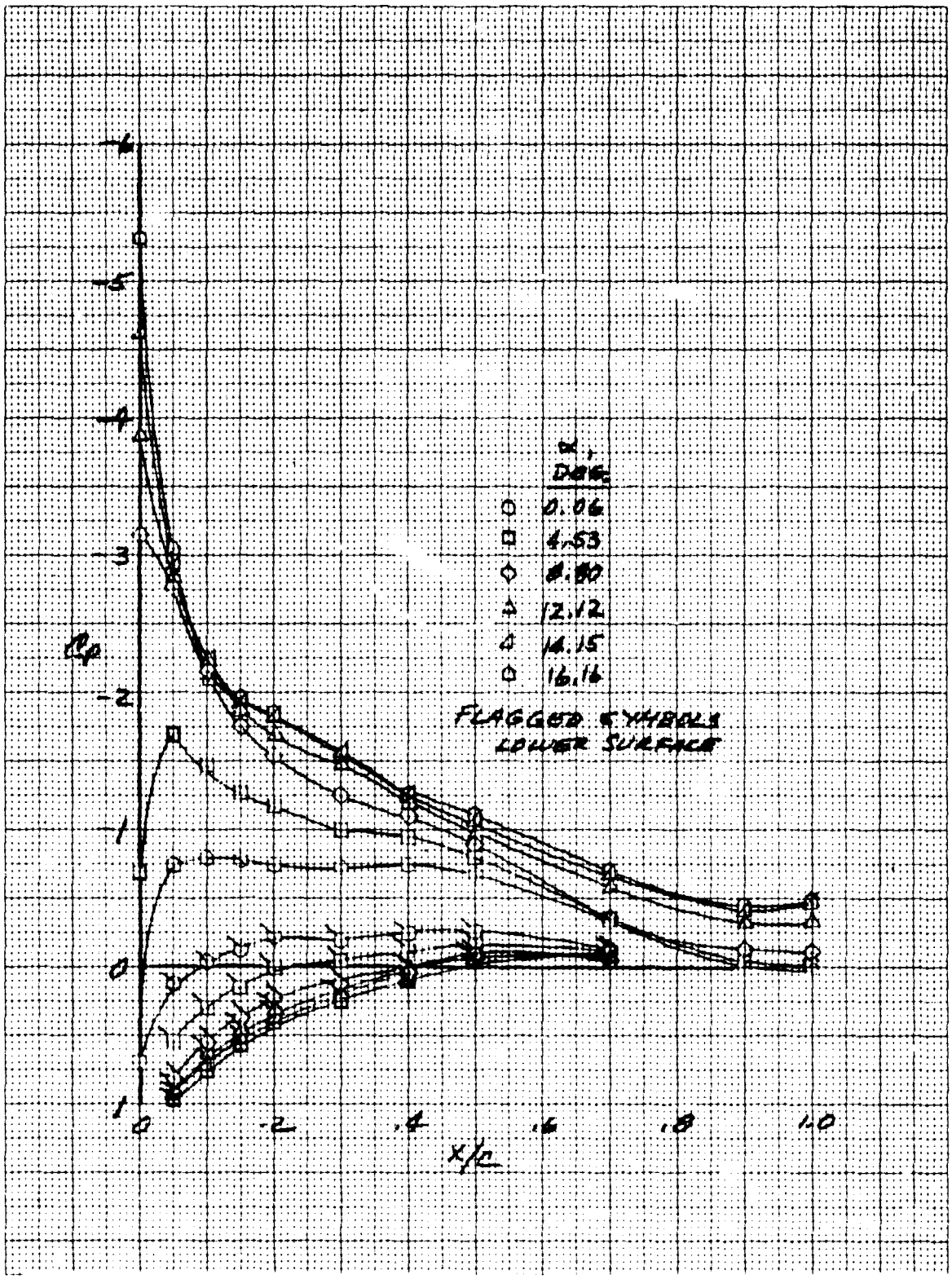

(b) Right-wing pressure strap 22.5 cm (9 in.) from fuselage centerline (inboard of nacelle).

Figure 23.- Concluded.

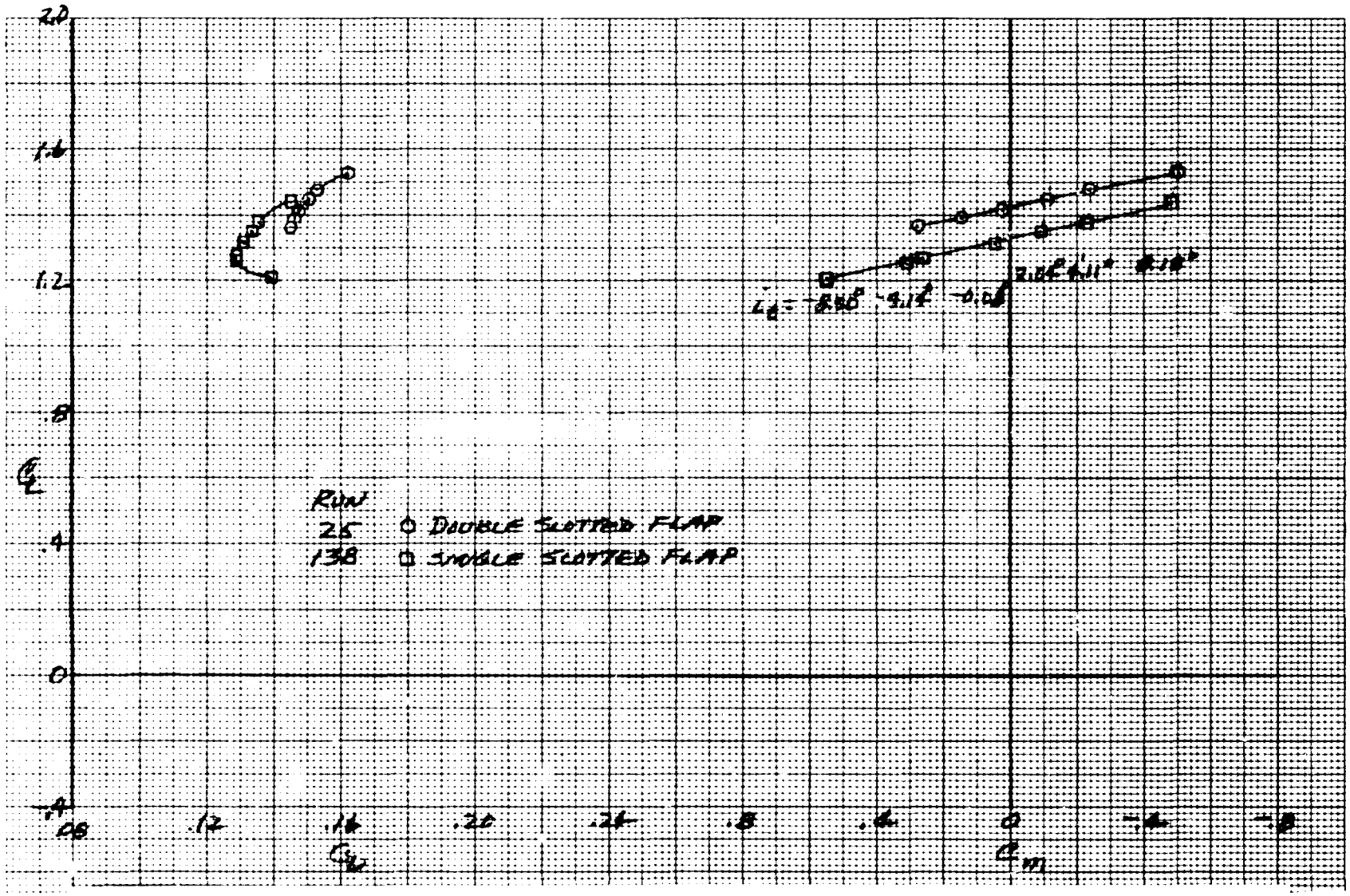

Figure 24.- Comparison of effects of tail incidence for two flap configurations; δ_f = 36°; α_u = 4°; q = 11881.5 N/m^2 (248.2 psf); Reynolds number = 1.618×10^6/m (5.31×10^6/ft).

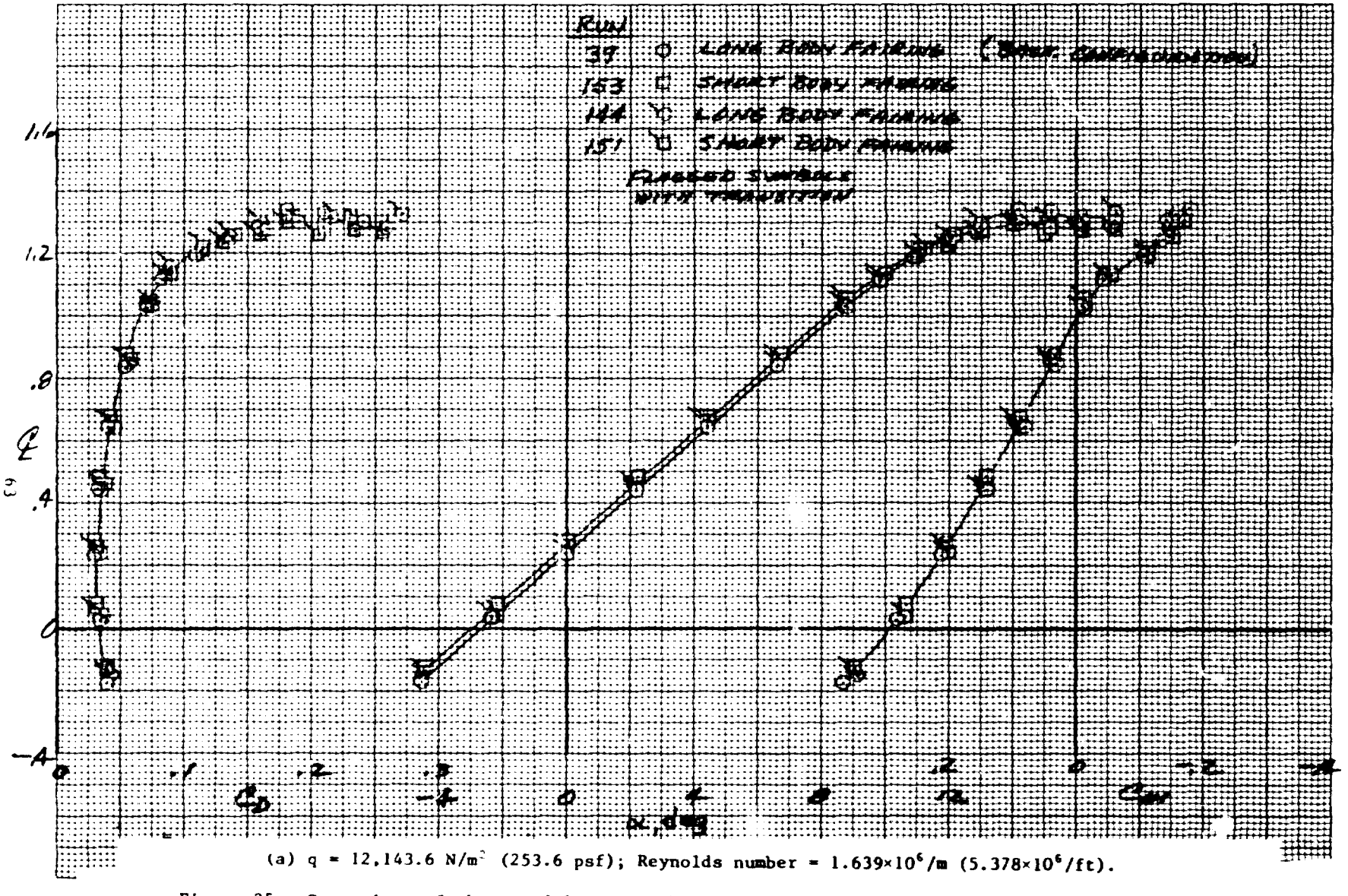

(a) q = 12,143.6 N/m² (253.6 psf); Reynolds number = 1.639×10^6/m (5.378×10^6/ft).

Figure 25.- Comparison of short and long wing-body fairing with and without transition; $\delta_f = 0°$.

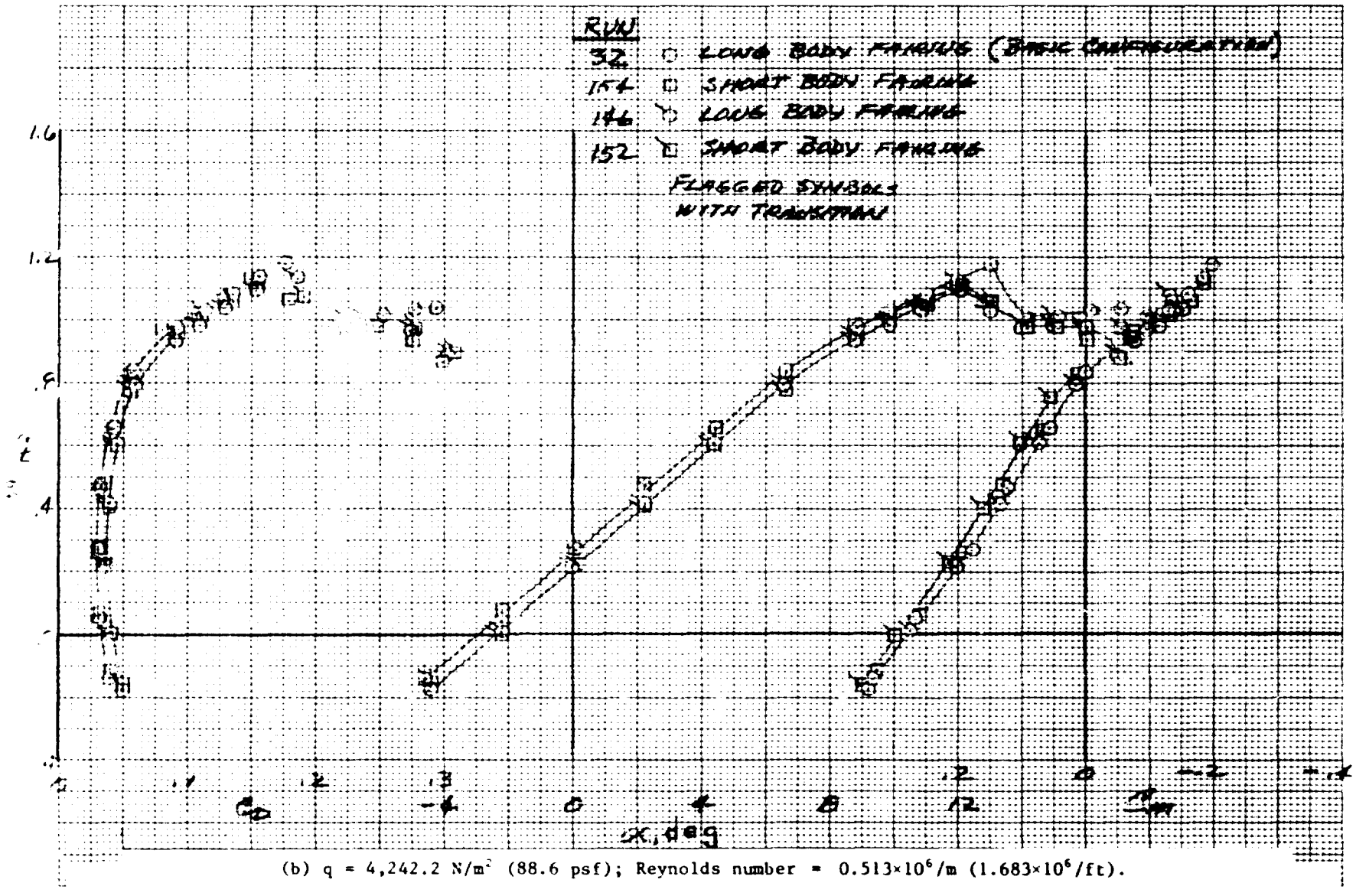

(b) q = 4,242.2 N/m^2 (88.6 psf); Reynolds number = 0.513×10^6/m (1.683×10^6/ft).

Figure 25.- Concluded.

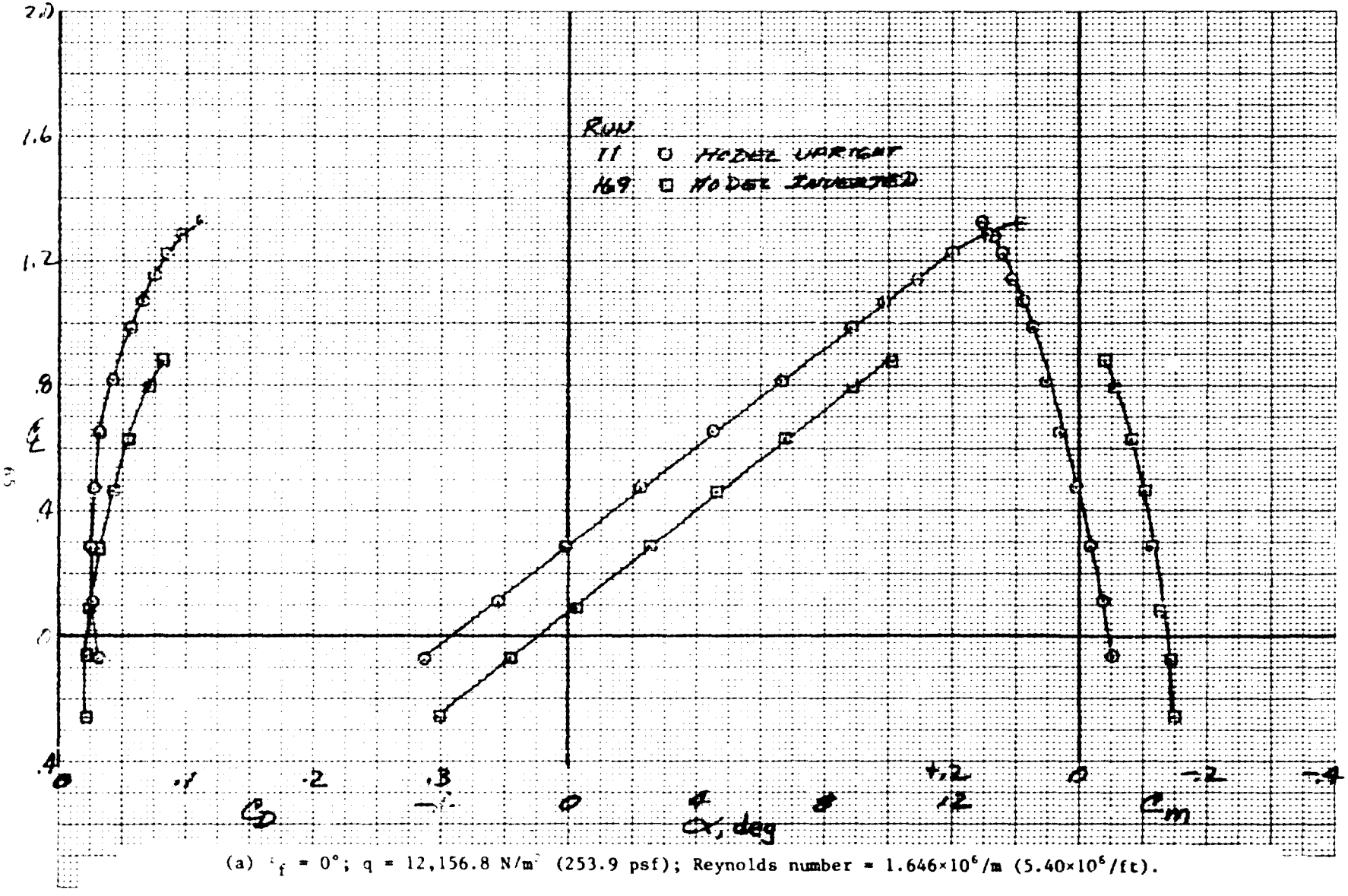

(a) $i_f = 0°$; q = 12,156.8 N/m² (253.9 psf); Reynolds number = 1.646×10^6/m (5.40×10^6/ft).

Figure 26.- Comparison of model mounting for wing-body configuration.

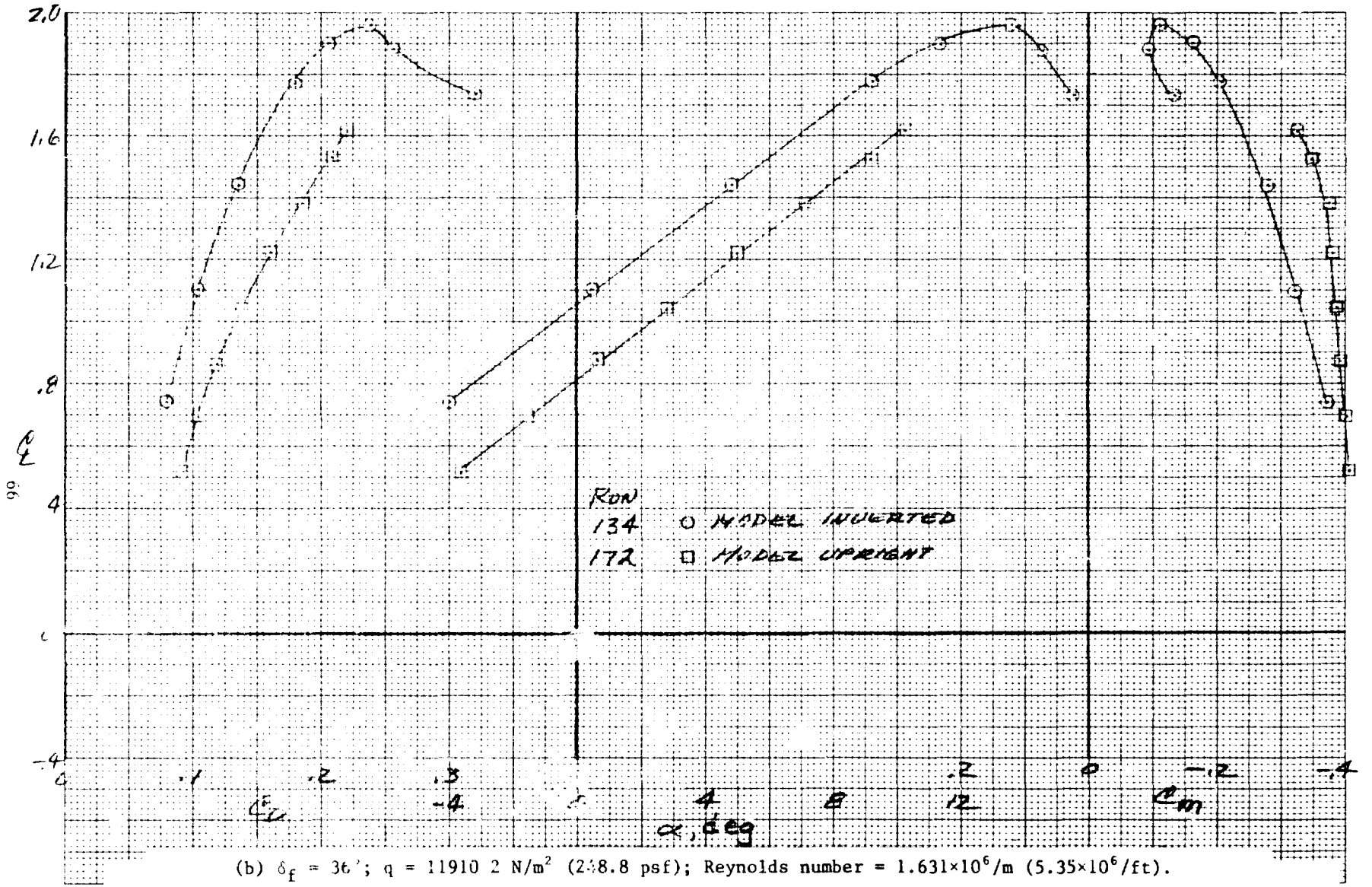

(b) δ_f = 36°; q = 11910.2 N/m² (248.8 psf); Reynolds number = 1.631×10⁶/m (5.35×10⁶/ft).

Figure 26.- Concluded.

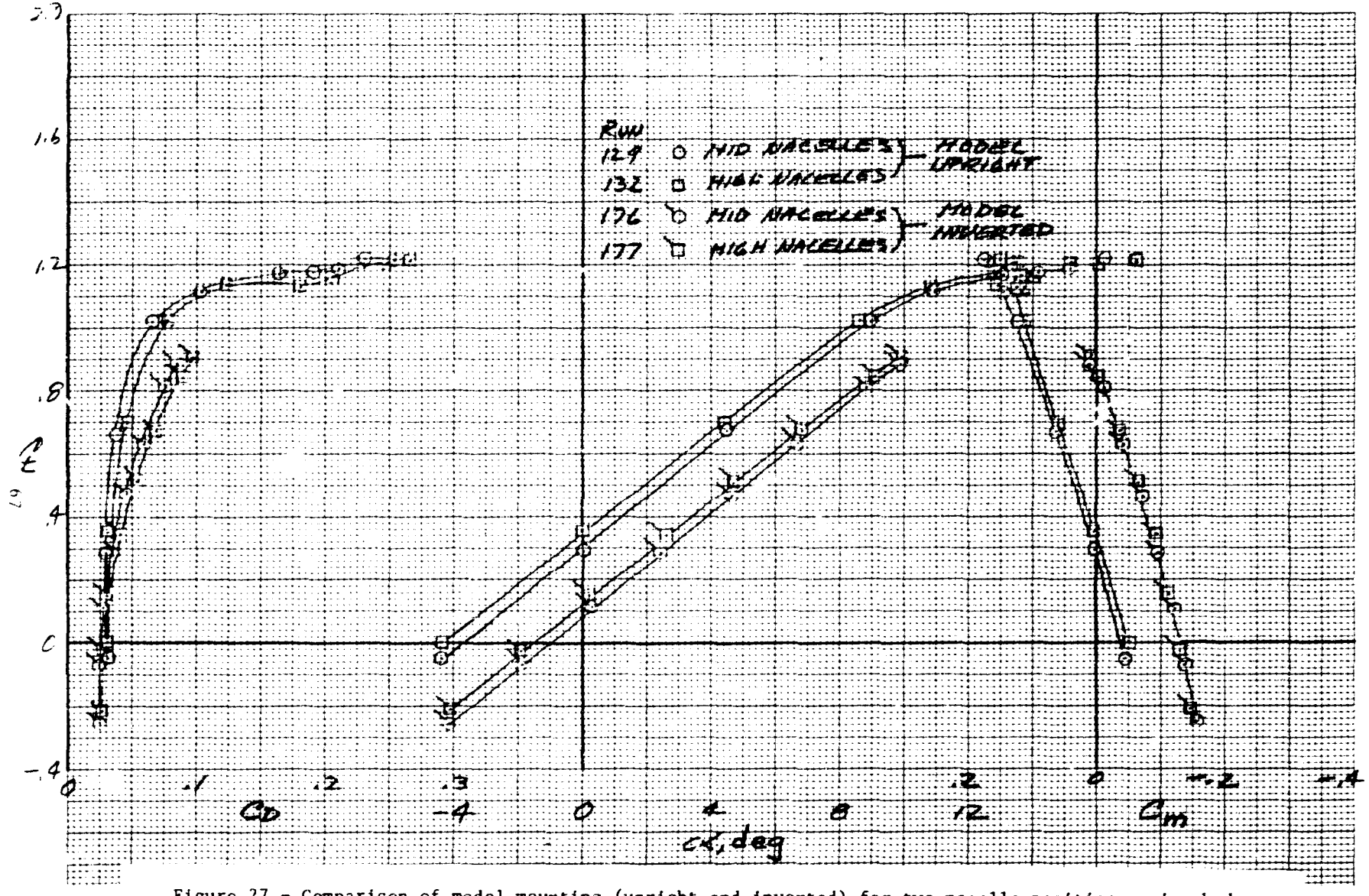

Figure 27.- Comparison of model mounting (upright and inverted) for two nacelle positions; wing-body-nacelle configuration; $\delta_f = 0°$; q = 11915.0 N/m^2 (248.9 psf); Reynolds number = 1.634×10^6/m (5.36×10^6/ft).

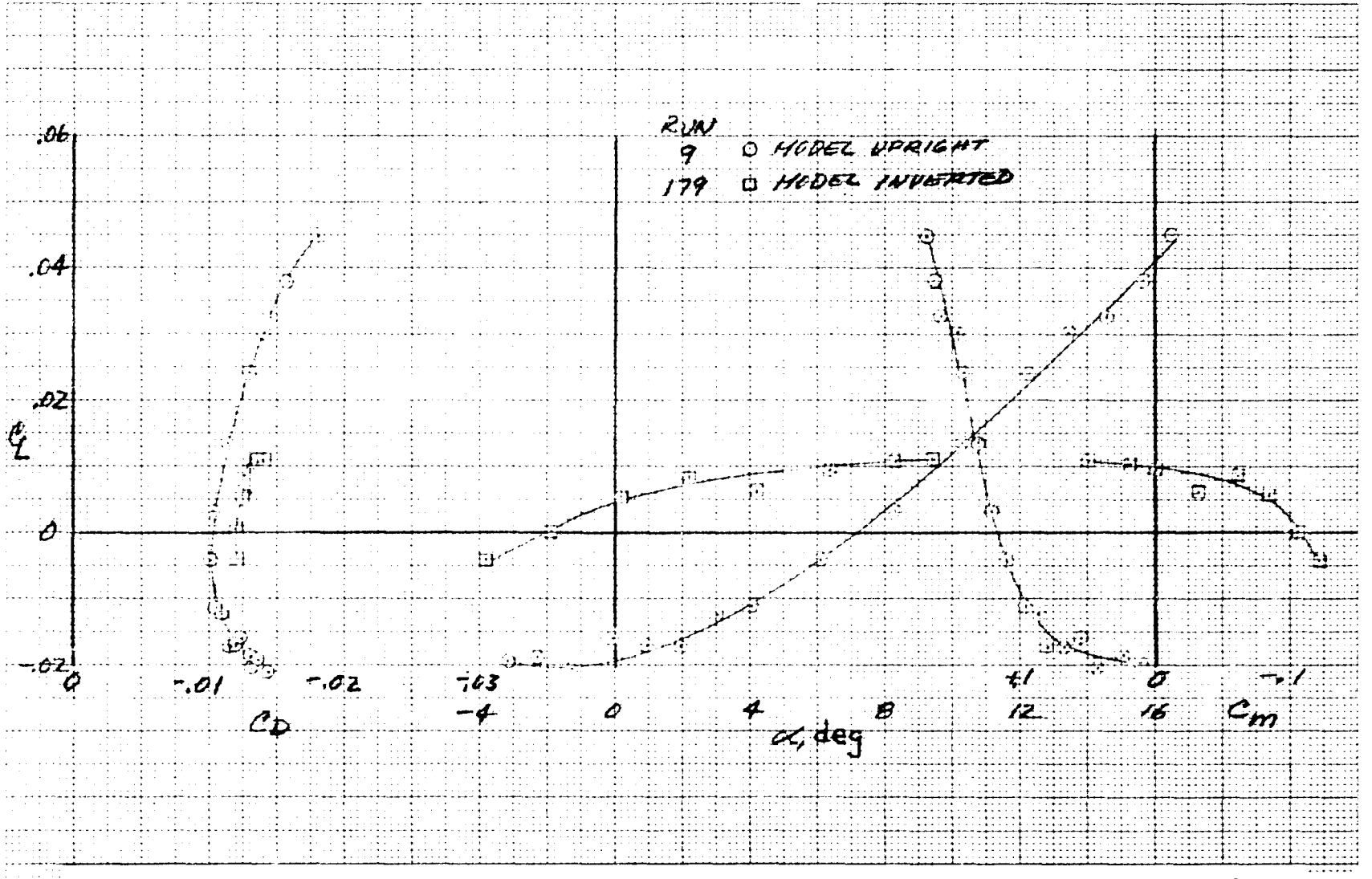

Figure 28.- Comparison of fuselage-only configuration mounted upright and inverted; q = 22111.1 N/m^2 (461.8 psf); Reynolds number = 2.131×10^6/m (6.99×10^6/ft).

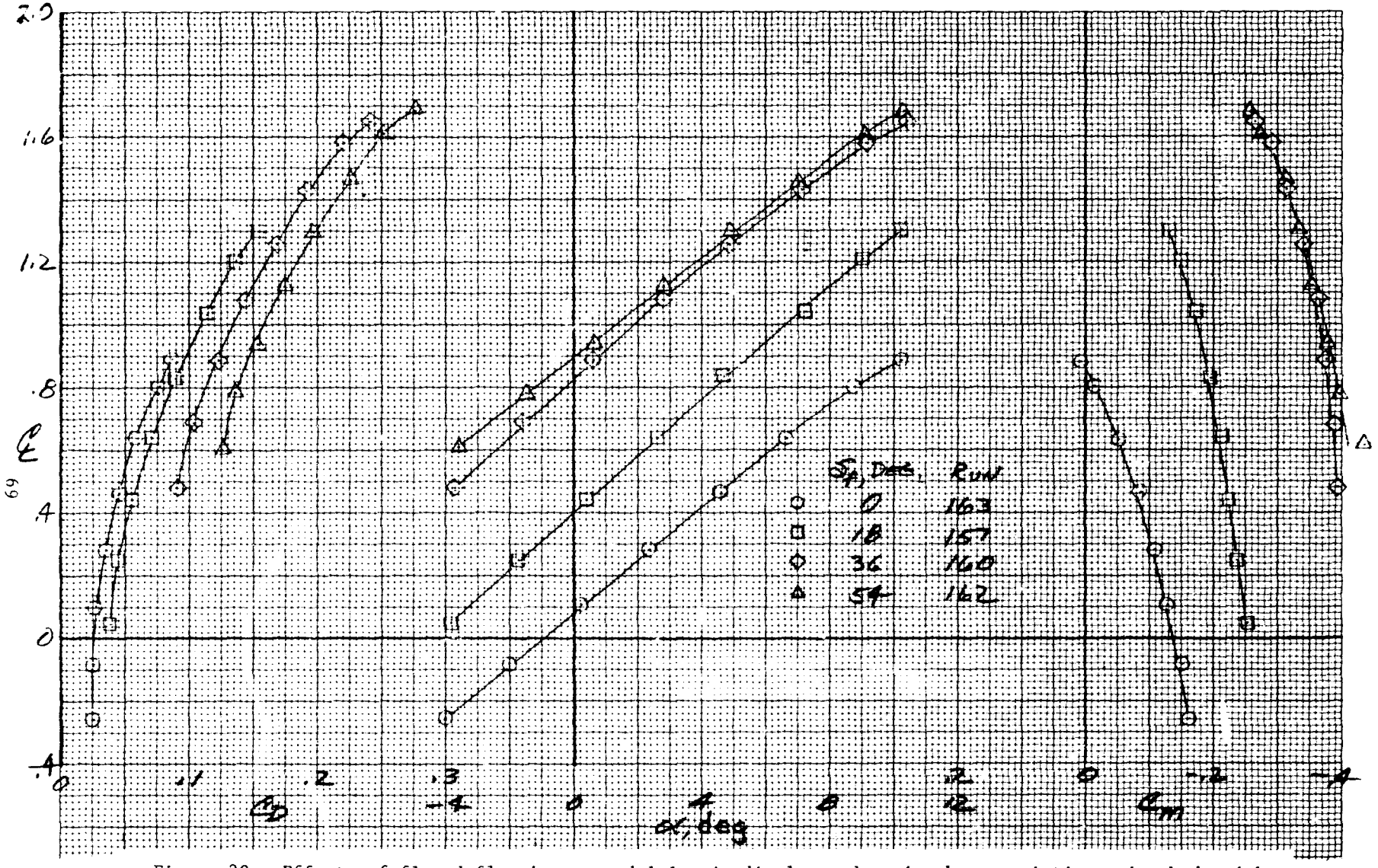

Figure 29.- Effects of flap deflection on model longitudinal aerodynamic characteristics; wing-body with full drooped-lead-edge configuration; model mounted inverted; q = 11968.9 N/m^2 (249.9 psf); Reynolds number = 1.634×10^6/m (5.36×10^6/ft).